ON THE ACOUSTIC RESPONSE OF ULTRASONICALLY – STIMULATED MICROBUBBLES AND ENHANCED INTRACELLULAR UPTAKE OF A FLUORESCENT MOLECULE

by

Shadab Momin

B. Sc., Ryerson University

Toronto, Ontario, Canada, 2013

A thesis presented to Ryerson University
in partial fulfillment of the requirements for the degree
of Master of Science in Biomedical Physics

Toronto, Ontario, Canada, 2016

AUTHOR'S DECLARATION

I hereby declare that I am the sole author of this thesis. This is a true copy of the thesis, including any required final revisions, as accepted by my examiners.

I authorize Ryerson University to lend this thesis to other institutions or individuals for the purpose of scholarly research.

I further authorize Ryerson University to reproduce this thesis by photocopying or by other means, in total or in part, at the request of other institutions or individuals for the purpose of scholarly research.

I understand that my thesis may be made electronically available to the public.

Shadab Momin

ABSTRACT

ON THE ACOUSTIC RESPONSE OF ULTRASONICALLY – STIMULATED MICROBUBBLES AND ENHANCED INTRACELLULAR UPTAKE OF FLUORESCENT MOLECULES

Shadab Momin

Master of Science, Biomedical Physics

Department of Physics, Ryerson University, 2016

Effectiveness of ultrasound-and-microbubble mediated therapy depends on the acoustic response of microbubbles. In this study, the acoustic response of microbubbles in the absence and presence of cells is measured using integrated cavitation dose (ICD) over harmonics/ultra-harmonics/broadband, and correlated with intracellular uptake of a fluorescent marker for varying peak-negative-pressures (PNPs). The ICD was independent of presence of cells. A PNP-threshold of 0.64 MPa was observed for microbubble's inertial cavitation; stable cavitation (PNPs<0.64MPa) and inertial cavitation (PNPs≥0.64MPa) regimes were identified. Within inertial cavitation regime, a stronger correlation (R^2>0.9) was observed between the ICD and FITC-positive cells, whereas, a weaker correlation, ranging from R^2=0.59 at 3rd ultra-harmonic to R^2 = 0.85 at 2nd ultra-harmonic, was observed under stable cavitation regime. The intracellular uptake, ICD and their correlation is dependent on microbubbles cavitation regime, indicating that ICD shows potential to predict bio-effects induced not only by inertial cavitation but also by stable cavitation of MBs.

ACKNOWLEDEMENTS

I would like to express my sincere gratitude to my supervisor, Dr. Raffi Karshafian, who pushed me to be a better researcher and showed me how to apply my knowledge beyond the scope of academics. Without his guidance, leadership and persistent help, I would not be able to complete my research. He also supported me in achieving my academic goals outside of research and encouraged me to be involved in different research projects.

I would also like to thank Dr. Jahan Tavakkoli and Dr. Yuan Xu, who have continuously offered their knowledge and expertise on my project. Their feedbacks not only helped me find ways to improve my research, but also helped me improve my research skills.

I would also like to thank Arthur Worthington, Graham Pearson, Matthew Forrest, Luke G, Iosif Deac, for their instantaneous support in resolving technical problems. I would like to thank Christopher Spring for his help with flow cytometry. I would like to thank Adriana Gaertner, and Tess Sy for all the administrative support. I would also like to show my appreciation thank Julia Pearse, Sheliza Jetha, Amin Sojahrood and Aren Ghabareki, who were co-operative and supportive at all times.

Finally, I would like to thank all the faculty members of the physics department at Ryerson University. Under the guidance of such knowledgeable and brilliant professors, the past seven years of undergraduate and graduate school has been a great learning experience. Thank you all.

Table of Contents

LIST OF ABBREVIATIONS

US – Ultrasound

MBs – Microbubbles

USMBs – Ultrasound and Microbubbles

PNP – Peak Negative Pressure

PRP – Pulse Repetition Period

PDP – Pulse Duration Period

PBS – Phosphate Buffered Saline

FDA – Food and Drug Administration

PCD – Passive Cavitation Detection

CD – Cavitation Dose

ICD – Integrated Cavitation Dose

TD – Time Domain

FFT – Fast Fourier Transform

PSD – Power Spectral Density

FITC – Fluorescein Isothiocyanate

LIST OF FIGURES

CHAPTER 1: INTRODUCTION

Microbubbles (MBs), currently utilized clinically as ultrasound contrast agents in diagnostic applications, are shell encapsulated gas filled bubbles with less than 5 μm in diameter (Kiessling et al., 2012). Experimentally, MBs are also being investigated for their applicability in therapeutic applications such as targeted drug and gene delivery. By acting as cavitation nuclei in the presence of ultrasound (US), MBs can create shear stress on cells and transiently permeabilize the cell membrane by a phenomenon known as sonoporation (Van et al., 2006). Some studies have shown that inertial cavitation (MB collapse) is required to induce a therapeutic effect (Fan et al., 2013; Hallow et al., 2006), whereas other studies indicated stable cavitation (linear and non-linear oscillation of a MB) as the mechanism of sonoporation (Forbes et al., 2011; Datta et al., 2008). Moreover, majority of studies designed to investigate MBs' cavitation dynamics for optimizing therapeutic applications are performed on a single MB (Forbes et al., 2011; Thomas et al., 2009) or on a population of MBs diluted in water or saline (O'Reilly et al., 2012). However, cavitation activities of a population of MBs under USMB therapeutic conditions and in the presence of cells may be different from that of a single MB in water alone or in the absence of cells.

Acoustically, MBs emit harmonic and ultra-harmonic energy during stable cavitation and a broadband spectrum upon inertial cavitation (Hoff, 2001). Previously, such cavitation activities of MBs has been quantified using Integrated Cavitation Dose (ICD), which was then correlated with bio-effects (Lai et al., 2006; Chen et al., 2003). The correlation of the ICD with hemolysis (Chen et al., 2003) and sonoporation (Lai et al., 2006) was found to be R^2=0.99 and R^2=0.75, respectively. Nevertheless, the correlation between the ICD and ultrasound-microbubble

(USMB) induced bio-effects is not well understood to be able to use the ICD as a predictor of USMB induced bio-effects.

In this study, we will characterize the acoustic behavior of a population of MBs in the absence and presence of cells at varying peak negative pressures (PNPs). In addition, USMB induced intracellular uptake of a fluorescent molecule will be measured and correlated with stable and inertial cavitation of MBs. MBs' acoustic response will be measured using Passive Cavitation Detection (PCD) method and quantified using Integrated Cavitation Dose (ICD) over the harmonics, ultra-harmonics, and broadband spectra.

1.1 ULTRASOUND (US) PHYSICS

Ultrasound (US) is a sound wave with a frequency higher than 20 KHz, the audible range by the human ear as shown in Figure 1.1. Although US is mainly used for diagnostic applications such as for detection of the blood flow and contrast enhancement (Schutt et al., 2003), recently, it has also been utilized for therapeutic applications such as drug and gene delivery and sonothrombolysis (Dijkmans, 2004). US is operated at frequencies ranging typically from 2 MHz to 18 MHz in diagnostic applications, whereas its frequency range in therapeutic applications has been reported to be between 20 KHz to 3 MHz (Fig 1.1) (Carovac, 2011; Nyborg, 1996). Therapeutic range of US can cause thermal and non-thermal biophysical effects involving the heating of the tissue and the combination of acoustic streaming and cavitation, respectively. Biophysical effects are classed as thermal (continuous wave and pulsed wave exposure) and non-thermal (pulsed wave exposure); this study involves the pulsed wave exposure. Physical characteristics of a pulsed US wave is shown in figure 1.2.

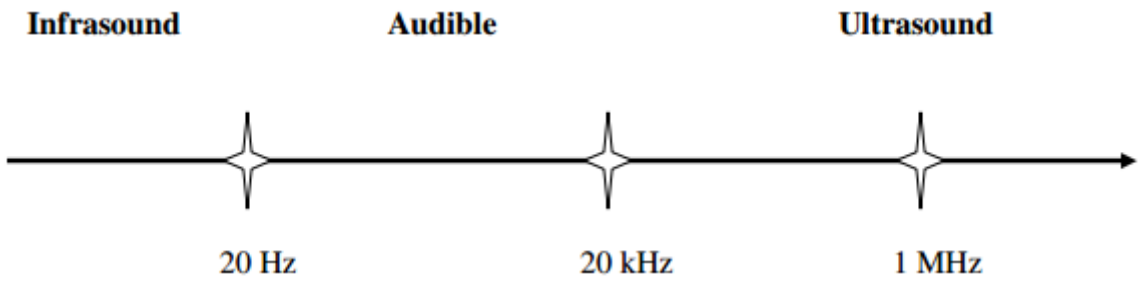

Figure 1.1: Different types of sound waves and their typical frequency range (Hafez, 2008).

1.1.1 Ultrasound Propagation

Two forms of acoustic propagation are transverse and longitudinal (Cobbold, 2007). A transverse US wave propagates by stimulating the particles or molecules of the medium perpendicular to the direction of the wave propagation. Whereas, a longitudinal US wave propagates longitudinally by stimulating the particles or molecules of the medium in the direction of wave propagation (Cobbold, 2007). In soft tissue or homogeneous medium, US acts as a longitudinal wave (Cobbold, 2007). This study involves longitudinal propagation of US in either degassed water or in the presence of cells.

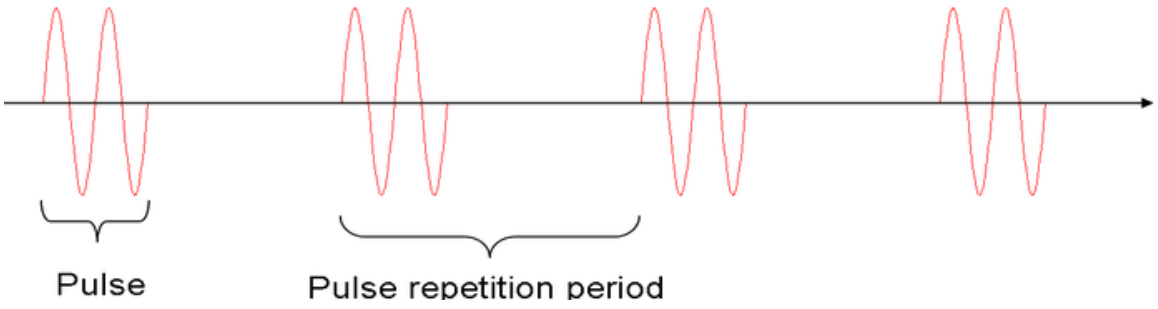

Figure 1.2: A representation of the physical characteristics of ultrasound pulsed wave indicating PRP number of cycles (n=2) and total number of pulses (N=4).

As energy propagates from one particle to the other, a longitudinal wave forms two alternate regions of compression and relaxation (Fig.1.3). Compression of molecules refers to the accumulation of energy, whereas relaxation refers to decrease in energy. The intensity in compressional and relaxation region of a longitudinal wave depends on the acoustic amplitude of the propagating wave. The speed with which an US wave propagates depends on the properties of the medium such as density and bulk modulus. Mathematically, it can be defined by the equation 1.1 where bulk modulus($\beta = -V\frac{dP}{dV}$) is the relative change in volume of the medium as pressure changes by dP (Cobbold, 2007).

$$c = \sqrt{\frac{\beta}{\rho}} = \sqrt{\frac{Bulk\ modulus\ of\ the\ medium}{density\ of\ the\ medium}} \qquad [1.1]$$

Both, diagnostics and therapeutics, applications of ultrasound involve the propagation of ultrasound waves into the tissue of the subject over a focused region. As a result, a propagating US wave will eventually interact with different organs and tissue along its path.

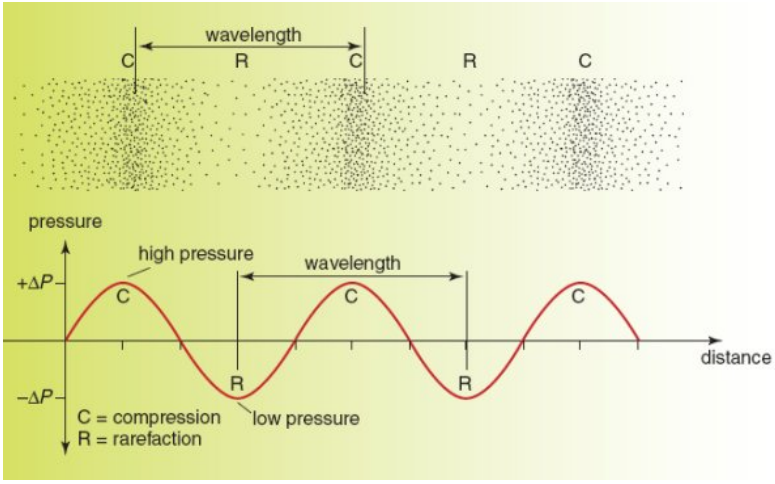

Figure 1.3: Schematic of ultrasound wave and the movement of the particles in the media as a function of compressional (C) and rarefactional (R) region. (Jacaranda Physics 1 2nd Eddison © John Wiley & Sons, Inc.)

1.1.2 Ultrasound interaction with matter

Ultrasound interaction depends on the characteristics of an US wave and physical properties of the medium (e.g., tissue or an object) through which US beam passes. The particles of the medium resist change due to mechanical stress caused by compressional and rarefactional region of an US wave. The resistance of the particles of the medium is referred to as the characteristic acoustic impedance of a medium, which is directly proportional to density of the medium and the speed of sound in the medium through which US beam propagates. It can be defined mathematically by equation 1.2

$$\mathrm{Z}\left[\frac{\mathrm{Pa.s}}{m^3}\right] = \rho\left[\frac{kg}{m^3}\right] c\left[\frac{m}{s}\right] \qquad [1.2]$$

When an US wave interacts with an object that has a different acoustic impedance than that of surrounding media, it is reflects due to acoustic mismatch. Reflection is the most important interaction process for producing an US image. The type of reflection depends on the size of the object relative to that of the ultrasound beam. Specular reflection occurs when an US interacts with an object that has smooth surface and a dimension greater than one wavelength of the US beam. In diagnostic US, this type of reflection is useful for recognizing fibrous structures such as tendons and boundaries between different tissues (Cobbold, 2007).

Non-specular reflection or scattering occurs when an US wave interacts with the reflecting interface that is irregular in shape and smaller in dimension than one wavelength of the US beam (Cobbold, 2007). In general diagnostic beams have a wavelength of 1 mm or less. Since the number of structures within the organs are less than 1 mm, this type of reflection provides important information about internal structures of organs for diagnostic purposes. This study relates only to the non-specular reflection as the dimension of the reflecting surface, microbubbles, is relatively small compared to the beam diameter. Scattering of US from a small

scatterer (a << λ) depends on variations in density and compressibility (Equation 1.3) (Cobbold, 2007).

$$p_s(r,\theta) = p_i e^{-jkr}\frac{k^2R^3}{3r}\left[\frac{k_v-k_0}{k_0}+\frac{3(\rho_v-\rho_0)}{2\rho_v+\rho_0}\cos\theta\right] \quad [1.3]$$

where p_s is the scattered peak pressure, p_i is the incident pressure amplitude, $k = {2\pi f}/{c}$ is the acoustic wave number and R = a/2 is the radius of the scatterer. The compressibility and density of the medium is denoted as k and ρ and subscripts v and o represents the scatterer and surrounding medium, respectively. The fractional change in compressibility given by the first term of the equation is the monopole term. Monopole radiation is the scattered pressure which arises from the scatterer when the density of the scatterer is the same whereas the compressibility is different than the surrounding medium. Whereas, the dipole term refers to the scattered pressure from the scatterer when the compressibility of the scatterer is the same but density differs (Nassiri et al., 1986). The dipole term causes the scatterer to undergo back and forth motion due to difference in the densities of the medium (Cobbold, 2007). The monopole term is more dominating term in most biological media such as scattering from RBCs and tissue and dipole term is neglected (Cobbold, 2007). Thus, US scattering from air/gas filled MBs plays an important role in many diagnostic applications of US. Furthermore, the combination of ultrasound and microbubbles (USMBs) have also shown induce beneficial bio-effects and it is currently under investigation for its applicability in drug/gene delivery (Dijkmans et al., 2004).

1.2 MICROBUBBLES (MBs)

Microbubbles, smaller than a red blood cell (RBC) in diameter, are air or gas filled bubbles that are encapsulated by a shell such as protein, lipid or polymer (Forbes, 2009). MBs are used in diagnostic applications to increase acoustic reflectivity to improve the contrast of US

images from deep tissues or small vessels. Currently, their applicability to improve therapeutic applications such as drug/gene delivery, thrombolysis and sonodynamic therapy is under investigation (Stride et al., 2010).

Initially, large sized free air bubbles were introduced for improving ultrasound images. However, a larger size (>10micrometer) and faster diffusion rate limited their applications because of their inability to transverse the pulmonary circulations. Smaller sized MBs were then introduced to extend the range of diagnostic applications (Carrol et al., 1980). Soon after, Echovist® and Levovist®, composed of galactose coating, were developed and approved in Canada for enhancing the right ventricle and left ventricle (Raisinghani et al., 2002). Furthermore, Albunex®, an air filled and human serum albumin encapsulated MB, was then approved in the US. All three MBs, however, were not able to persist longer in the presence of US because they contained air as the gas. Thus, Albunex® was redesigned with perfluorocarbon gas to increase its longevity (Raisinghani et al., 2002). Another example of perfluorocarbon gas filled MB is Definity® that is approved in Canada and USA as an IV injectable MB and currently being used in echocardiography (Raisinghani et al., 2002). Ostwald coefficients determine the rate at which MBs radius decreases by measuring the rate of MBs disappearance (Raisinghani et al., 2002). Lower the Ostwald coefficient, longer it takes for a gas to diffuse (Raisinghani et al., 2002). The disappearance time of air and perfluoropropane gas is 0.02 and 1.1 seconds, respectively (Correas et al., 1997; Quaia et al., 2005).

In addition to diagnostic applications of MBs, currently, their applicability to improve therapeutic applications such as drug/gene delivery, thrombolysis and sonodynamic therapy is under investigation (Stride et al., 2010). Both, therapeutic and diagnostic, applications of MBs

depend on acoustic properties of MBs, which, to some extent, are influenced by their characteristics.

1.2.1 MB's characteristics

In general, MBs are less than 5 μm in diameter allowing them to pass through smallest blood vessels. It consists air or a gas such as perfluorocarbon, sulfur hexafluoride or perfluorten. It is encapsulated by a shell such as lipid, polymer, albumin or protein.

The use of MBs in diagnostic and therapeutic applications depends on aforementioned physical characteristics. For instance, smaller sized MBs (smaller than a RBC) are used to trace pulmonary microcirculation from right to left heart (Hernotd et al., 2008). Secondly, shell encapsulation around a free gas bubble increases the effects of surface tension and decreases the diffusion rate of the entrapped gas. Because the shell adds the stiffness effects to MBs, it becomes more resistant to distortion compared to that of free gas bubbles. Under the same US exposure condition, thick shelled (0.5 – 1.2 μm) MBs are more stable compared to that of thin lipid shelled (1 – 5 nm) MBs. Thus, loading drugs into a thick shelled MBs may be beneficial for targeted drug delivery chemotherapeutic drugs to reduce the side effects (May et al., 2002). Quantison™ MB is encapsulated by a human serum albumin, which is highly stiffed compared to lipid. Definity® is an example of a lipid encapsulated MB. At lower acoustic pressures, Definity® have shown to provide larger scatter than Quantison™ (Sboros et al., 2003). Thin lipid shelled MBs, therefore, are often used in ultrasonic imaging (May et al., 2002). They are also preferred in drug delivery because they are less resistant to fragmentation, which plays a critical role in many therapeutic application. Thus, lipid shelled MBs are more frequently used in drug delivery application.

In this study, Definity®, a lipid shelled and octafluoropropane gas filled MB, is used. Definity® MBs are approved by US FDA as an IV injectable MB and are currently being used in echocardiography. It has concentration of approximately 1.20×10^{10} MBs per millilitre. The mean diameter of Definity is 1.1 – 3.3 μm and about 98% of MBs are less than 10 μm in size (Evan et al., 2003).

1.2.2 Interaction of MBs with Ultrasound (US)

Microbubbles undergo a wide range of complex behavior upon interaction with an US wave. In general, MBs act as cavitation nuclei by contracting and expanding in responds to peak compressional and rarefactional region of an US wave. MB behavior depends on US parameters (e.g., acoustic pressure, acoustic frequency, PDP, PRP), physical condition of the surrounding medium (e.g., viscosity, temperature) and MBs physical characteristics. However, among all, the acoustic pressure has the biggest impact on MB behavior (Sboros, 2008). In general, MBs cavitation has been categorized into two regimes: stable cavitation and inertial cavitation.

Linear oscillation

MB exhibits a linear oscillation at low acoustic pressure and generate US signals with the transmitted frequency (f). During linear oscillation, the amount of MB's contraction and expansion is the same (Hoff et al., 2001). This type of MB response is controlled by compressibility of the entrapped gas and inertial force of the surrounding fluid on the MB surface. Linear oscillation of a free gas MB, neglecting the surface tension, is similar to that of damped oscillator (Equation 1.4). The damped oscillator can be further used to describe a microbubble in a fluid environment (i.e., water) in which the gas core acts as the spring and the surrounding fluid acts as the mass. The spring constant and the mass are replaced by equation 1.5

a and 1.5 b (Forbes, 2009). Substituting equation 1.5 a and 1.5 b into equation 1.4 gives equation 1.5 c, which represents the resonance frequency of a MB (Forbes, 2009).

In a mass spring system		***In a free gas MB system***	
$w^2 = \frac{k}{m}$	[1.4]	$k = 12\,\pi\,\kappa\,R_0\,P_0$	[1.5 a]
k = the spring constant		$m = 4\pi\,R_0^2\,\rho$	[1.5 b]
m = mass of the spring		$\omega_0 = \frac{1}{R_0}\sqrt{\frac{3\,\kappa\,P_0}{\rho}}$	[1.5 c]

In a free gas bubble system, κ represents the polytropic gas constant, R_0 represents the equilibrium bubble radius, P_0 represents the pressure of the surrounding fluid on MB surface, ρ represents the density of the surrounding medium and ω_0 represents the resonance frequency of a MB. As shown by equation 1.5 c, MB radius is inversely related to the resonant frequencies of a MB. Thus, the resonance frequency of a MB decreases with radius.

Non-linear oscillation

As the acoustic pressure amplitude increases, MB behavior gradually shifts towards the non-linear oscillation. At higher acoustic pressures, USMB contracts at a higher rate but it can only contract until compressibility of entrapped gas reaches its maximum. Thus, MBs become more resistant to contraction than to expansion during non-linear oscillation. During non-linear oscillation, MB generates non-linear and asymmetrical US signals at the transmitted frequency (f) or higher order harmonics (2f, 3f, 4f, etc.,) or ultra-harmonics ($\frac{3}{2}$f, $\frac{5}{2}$f, $\frac{7}{2}$f, etc.,) (Quaia, 2005). On the other hand, the expansion occurs slowly during the rarefactional region of the ultrasound wave (Fig 1.4).

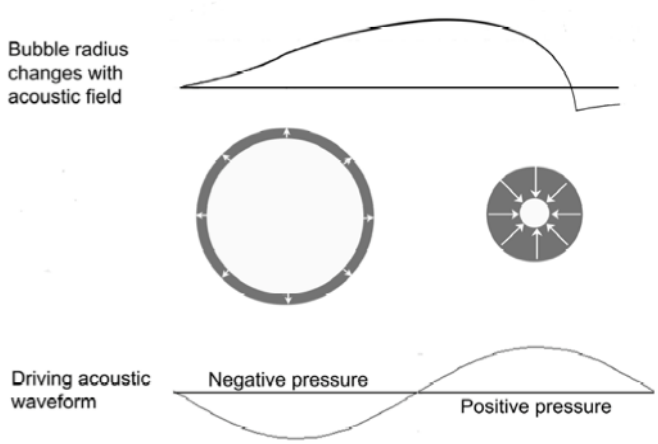

Figure 1.4: Bubble radius as a function of peak rarefactional and compressional acoustic pressure. (Forbes, 2009)

For non-linear oscillations of MBs, the energy lost due viscosity of the surrounding fluid can be added to the linear Rayleigh-Plesset model (Forbes, 2009; De Jong et al., 2009).

$$\mathrm{p}_l R R^{00} + \frac{3}{2}\mathrm{p}_l R^{o\,2} = \left(p_0 + \frac{2\sigma}{R_0}\right)\left(\frac{R}{R_0}\right)^{-3k}\left(1 - \frac{3k}{c}R^0\right) - \frac{2\sigma}{R} - \frac{4\mu R^0}{R} - p_0 - P(t) \quad [1.6]$$

Where

R = Microbubble Radius

R^o = 1st Time Derivative of Radius (the velocity of the microbubble wall)

R^{oo} = 2nd Time Derivative of Radius (the acceleration of the microbubble wall)

μ = The shear viscosity of the medium.

σ = Surface tension

p_l = Density of medium

p_0 = Ambient pressure

$P(t)$ = Applied acoustic pressure field

k = Polytropic gas constant

c = Speed of the sound

Inertial Cavitation

Microbubble fragmentation occurs at higher acoustic pressures. Under this condition, MBs expands moderately and contracts rapidly that the change in MB radius with time reaches the speed of sound (Forbes, 2009). When a MB collapse occur due to inertial forces, an increasing amounts of kinetic energy is transferred to the contracting MB (Chomas et al., 2001). When pressure force dominates the inertial force, MB collapses in the expansion phase. It has been reported that MB experiences inertial cavitation when MB radius reaches twice of its equilibrium radius during expansion (Forbes, 2009). Previously, a study has shown that the maximum radius, R_{max}, of MB during expansion before fragmentation can be up to five times greater than its equilibrium radius, R_0. (Chomas et al., 2001). When a shell encapsulated MB collapses, it generates a free gas MB which can also oscillate and collapse. Acoustically, a broad band signal is emitted by a collapsing MB. (Quaia, 2005). Furthermore, MB collapse also result in rapid increase in harmonics and ultra-harmonics amplitudes (King D.A. et al., 2010).

1.3 CHARACTERIZATION AND QUANTIFICATION OF MBs' CAVITATION ACTIVITIES

In the presence of US, MBs' cavitation activities can be characterized into two categories: stable cavitation and inertial cavitation. Such cavitation activities of MBs in response to ultrasound can be characterized by using acoustic and optical methods. Optical method provides a very clear insight about change in cavitation activities over a period of time. The optical methods are normally used to study the physical behavior of MBs such as oscillations, rebound, fragmentation and production of free gas bubbles during ultrasound exposure (King D.A. et al., 2010). However, this technique is normally used for a single MB. Furthermore, the drawbacks of using this method are limitation of temporal and spatial resolution, limited size of

data set and expense involved in the necessary equipment. In present study, an acoustic method known as passive cavitation detection (PCD) is used to record the cavitation activities of MBs. The advantage of acoustic measurements is that it records the cavitation activities as an average response from a population of MBs.

1.3.1 Passive Cavitation Detection (PCD) method

PCD includes a detector, an ultrasound transducer or a hydrophone, which passively listens to the MBs' acoustic emission. Through this method, the linear and non-linear response during MBs' stable cavitation can be distinguished via spectral analysis. In terms of inertial cavitation, it is generally agreed that a large amplitude acoustic response of MBs and emission of broadband spectrum are closely linked with the inertial cavitation (Chomas et al., 2001). Using PCD, a previous study determined inertial cavitation threshold pressure for a single Definity® MB by identifying post excitation collapse signal in time domain (A. King et al., 2010). Since PCD records the cavitation events during US insonication, the cavitation stage of MBs during US insonication can be identified via spectral analysis. In present study, cavitation activities of Definity® MBs will be quantified using the integrated cavitation dose (ICD) method. The ICD is typically quantified by integrating the area under a specific frequency window of scattered echoes (Qiu et al., 2010; Chen et al., 2003; Lai et al., 2006). The ICD method used in this study is delineated in chapter 2 and will be used to determine a range of PNPs for stable cavitation and inertial cavitation of Definity® MBs. Similar approach has been used in the past to identify the PNP-threshold for inertial cavitation of Optison®, biSpheres® and Sonazoid® MBs (Chen et al., 2003).

1.4 US AND MBs MEDIATED THERAPEUTIC APPLICATIONS

Ultrasound-and-microbubbles (USMB) have been utilized in targeted drug delivery applications where it has been shown to improve therapeutic effect of chemotherapeutic agents in both *in vitro* and *in vivo* models (Nelson et al., 2002; Liu et al., 2006). The underlying mechanism appears to be partly associated with enhanced uptake of molecules (e.g. Cisplatin, Gemcitabine) mediated through the shear-stress generated by stable and inertial cavitation of MBs (Postema et al., 2004). There are two aspects that may play a role in the efficacy of USMB mediated drug delivery applications: the acoustic response of MBs and the associated cellular physiology (Baker et al., 2001). USMB has been shown to enhance intracellular concentration of drugs/molecules through sonoporation, endocytosis and fluid phase uptake.

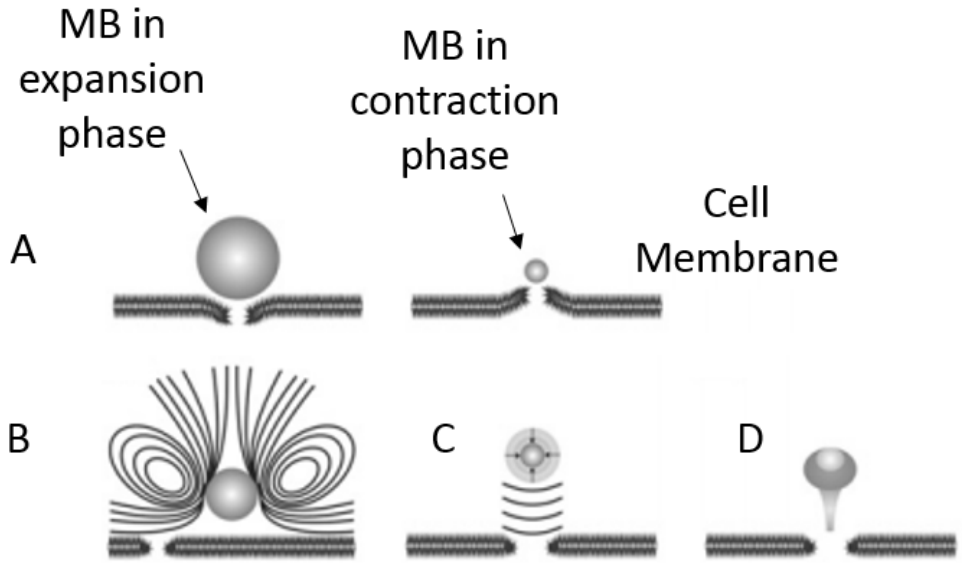

Figure 1.5: Biophysical effects created in the environment by different acoustic mechanisms of MBs and their effects on the cell membrane. (A) MB's contraction and expansion (Stable cavitation) (B) micro-streaming generated by stable cavitation, (C) shock wave generated by MB's collapse and (D) liquid jet created by MB's collapse near the surface. Adapted and modified from Lentacker et al., 2014.

The acoustic response of microbubbles depends on the US exposure conditions such as pressure and frequency, the microbubble characteristics such as size and shell properties, and the environment (Brenan, 2013). A microbubble in the vicinity of a cell, when exposed to ultrasound, disturbs the integrity of the plasma membrane by exerting a pushing and pulling force and shear-stress through MB stable oscillation (Fig. 1.5 A, B) (Kotopolis et al., 2013). Furthermore, a collapsing microbubble can generate a shockwave and liquid-jet disrupting the cell membrane (Fig. 1.5 C, D) (Kotopolis et al., 2013).

It has been shown that both, stable and inertial cavitation, are capable of inducing sonoporation. For instance, it was optically shown for a single MB attached to the surface of the cell that inertial cavitation of microbubble was the most efficient in sonoporation (Fan et al. 2013; Fan et al., 2012), whereas others indicated stable cavitation as the mechanism of sonoporation (Forbes et al., 2011; Guzman et al., 2001). Different conclusions have been made regarding acoustic mechanism responsible for sonoporation. This may be due to our poor understanding of MBs cavitation dynamics. MBs' cavitation is affected by ultrasound parameters such as transmit frequency, acoustic pressure, pulse duration period, physical characteristics of MBs and surrounding fluid environment. Majority of studies designed to investigate MBs' dynamics for improving therapeutic applications are conducted with a single MB diluted in water or saline. Previously, the acoustic cavitation response of a single encapsulated MB (Definity® and Optison®) was characterized in the absence of cells (or in water only) at varying acoustic pressures (4 kPa to 4.1 MPa) to determine collapsing threshold pressure. Acoustic responses were then directly compared to the levels of sonoporation generated at each acoustic pressure (Forbes et al., 2011). However, cavitation activities of a population of MBs under USMB therapeutic conditions and in the presence of cells may be different from that of a single MB or

in the absence of cells. In this study, acoustic behavior of Definity® MBs as a population will be characterized in the absence and presence of cells.

As mentioned in previous chapters, MBs emit harmonic and ultra-harmonic energies during stable cavitation (linear/non-linear oscillations of MBs) and a broadband acoustic emission upon inertial cavitation (i.e., MB collapse). Using such spectral characteristics of backscattered signal, a parameter referred as integrated cavitation dose (ICD) was introduced to quantify MBs' cavitation activities (Chen et al., 2003). The ICD assesses the amount of cavitation activities by integrating the area under a specific frequency window of scattered echoes (Chen et al., 2003). In the past, the ICD was correlated with the percentage of hemolysis produced *in vitro* only for inertial cavitation activity of Optison® MBs; the ICD was quantified by integrating the area between 3.94 and 4.14 MHz while transmitting with 1.15 MHz center frequency (Chen et al., 2003). In another study, the relationship between sonoporation rate and the ICD was correlated only for inertial cavitation causing acoustic pressures; the ICD, here, was quantified by integrating ±500 KHz area under 10^{th} harmonic (Lai et al., 2006). In other study, the ICD was quantified by integrating the area between 2^{nd} and 3^{rd} harmonic and correlated with DNA-transection (Qiu et al., 2010). Studies aforementioned investigated this correlation mainly for inertial cavitation of MBs, which may be detrimental to the cells due to transient increase of local temperature and pressure (Liang et al., 2010). Deleterious effects also may be due to unrecovered pores on the cell membrane, which are relatively large for inertial cavitation compared to those formed by stable cavitation (Lentacker et al., 2014). Thus, currently, there is a need of MBs' cavitation quantification method such as the ICD that can predict acoustic bio-effects induced by stable or inertial cavitation of MBs. However, the correlation between the ICD and bio-effects is also not clearly understood due to numerous reasons. One of which is that

there is only a handful of studies that have investigated the correlation between the ICD and bio-effects. Secondly, this correlation, to our knowledge, has not been investigated for stable cavitation of MBs, which has previously shown significant uptake of fluorescence molecule at acoustic pressures below collapsing threshold (Forbes et al., 2011; Guzman et al., 2001).

Given that the ICD is quantified by integrating the area under a given frequency window, the same approach can be used to quantify the ICD for nonlinear oscillations of MBs as it generates higher harmonic and ultra-harmonic energies. In present study, the ICD was quantified over harmonics ($2f_0$, $3f_0$) and ultra-harmonics ($5/2f_0$, $7/2f_0$) and broadband spectrum (summation of harmonics and ultra-harmonics) for both stable and inertial cavitation regimes of MBs. We then correlated the ICD over harmonics, ultra-harmonics and broadband spectrum with intracellular uptake of a fluorescent molecule, with the goal of identifying its reliability not just for inertial cavitation but also for stable cavitation of MBs.

1.5 THESIS OUTLINE

This study is guided by the hypothesis that the integrated cavitation dose (ICD) is correlated with the intracellular uptake for both stable and inertial cavitation events of MBs.

The three specific objectives to test this hypothesis are:

- To quantify cavitation activities of MBs at varying PNPs in the presence and absence of cells using ICD and identifying PNP regime for stable and inertial cavitation of MBs.
- To investigate the effects of PNPs on intracellular uptake of Fluorescein Isothiocyanate (FITC – dextran).
- To determine the correlation between the ICD quantified over broadband/harmonics/ultra-harmonics frequencies and intracellular uptake of FITC-dextran without, and with considering MBs cavitation regime, respectively

In the first chapter, the US physics, MBs characteristics, USMB mediated therapeutic application, sonoporation and limitation of its applicability and thesis outline including hypothesis and specific objectives are discussed. In second chapter, the Passive Cavitation Detection (PCD) setup, a step by step procedure of ICD quantification and methods of analysis are described. Third chapter shows the result of acoustic behavior of MBs in the absence and presence of cells, the effects of peak negative pressure (PNP) on USMB induced intracellular uptake. Finally, the ICD and intracellular uptake is correlated for stable and inertial cavitation activities of MBs. The fourth chapter discusses the results of chapter three, conclusion, limitation of the present study and direction for future work. Chapter five includes the references and appendix with inclusion of additional descriptive plots/data for US equipment used in the present study.

CHAPTER 2: MATERIALS AND METHODS

Cells are exposed to ultrasound-and-microbubbles (USMB) in the presence of a fluorescent molecule at varying ultrasound pressures. During exposure, the acoustic response of microbubbles was measured using passive cavitation detection (PCD). Following exposure, intracellular uptake of a fluorescent molecule was measured using flow cytometry. Subsequently, the relationship between MB's acoustic response and enhanced intracellular uptake of a fluorescent molecule was assessed.

2.1 IN VITRO CELL MODEL

A human epithelial breast cancer cell line (MDA-MB-231, ATCC, MD, USA) was used in this study. The MDA cells were cultured in RPMI-1640 media with 10% fetal bovine serum (FBS), grown in a 37^{o}C incubator with 5% CO_2 and removed from flasks using trypsinization. The concentration of cells used in combination with ultrasound and microbubbles was kept constant at 1.0×10^6 cells per 1.5 mL volume for all experiments. The cells were suspended in RPMI cell culturing media at room temperature during the experiment.

2.2 CELL PERMEABILITY

The intracellular uptake, following ultrasound-microbubble exposure, was measured using 70 kDa Fluorescein Isothiocyanate, FITC-dextran, (FD500s, Sigma – Aldrich Co., St. Louis, MO), which has stokes radius of approximately 6 nm (Erickson et al., 2009). Prior to USMB, a 40 μL of FITC at a concentration of 3 mg/mL was added to a 1.5 mL cell suspension sample. Post USMB, samples were washed twice with phosphate buffered saline (PBS) and fixed with 2% paraformaldehyde (PFA); followed by two final washes and stored overnight at

4°C. The percentage of FITC positive cells was measured using BD FACSDIVA™ SOFTWARE (BD San Jose, California, USA). FITC-dextran has a maximum excitation of 490 nm and an emission of 520 nm.

Flow cytometry (BD LSRFortessa X-20, San Jose, CA) was used to assess the intracellular uptake. Post exposure, the cellular debris and aggregates were separated from each other by size using forward scatter area (FSA) and side scatter area (SSA) detectors. The values of FSA and SSA are measurements of voltage intensity set in the software that runs the flow cytometry. The population of MDA cells was assessed to be either permeable or impermeable to FITC dextran and measured in terms of percentage (Fig 2.1). Figure 2.1 shows the permeabilized FITC positive cells in a control and an US treated sample. The percentage of FITC positive cells are 0.3% and 32.2% in a control (FITC only) and a 1.12 MPa US treated sample with FITC and Definity®, respectively.

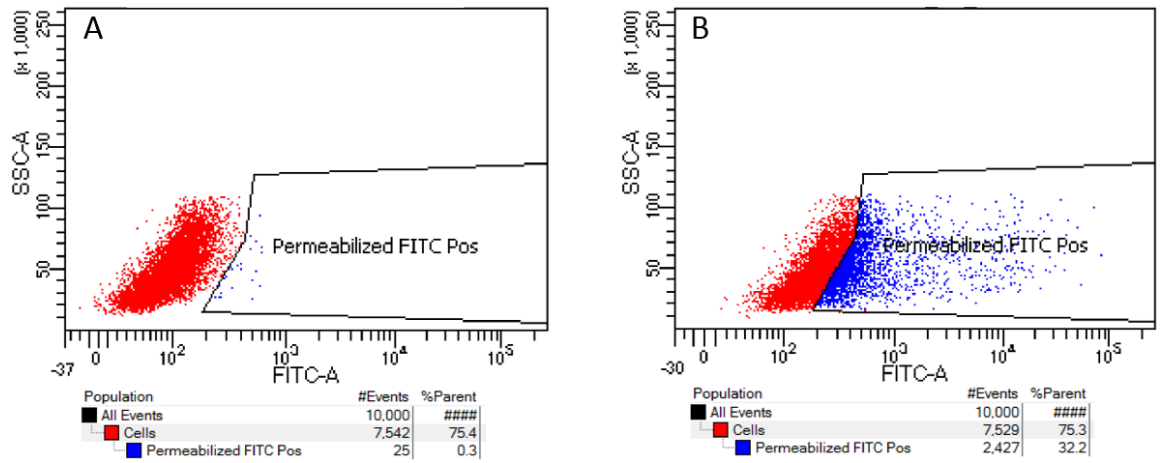

Figure 2.1: Dot plots of forward (FSC – A) and side (SSC – A) scattered of permeabilized FITC positive cells from (A) a control sample with FITC only and (B) a sample with FITC dextran, MBs and 1.12 MPa of US treatment.

2.3 DEFINITY®, MICROBUBBLE AGENT

Definity® (Lantheus Medical Imaging, Billerica, MA, USA) microbubbles were used in this study. Definity® are FDA approved for diagnostic application to opacify the left ventricular chamber and for distinguishing left ventricular endocardial border (Miller et al., 2008). It contains octofluoropropane (C_3F_8) gas and is encapsulated by a phospholipid shell. The reported mean diameter range of Definity® is 1.1 to 3.3 µm, with 98% of MBs having a diameter less than 10 µm. The initial concentration of Definity® MBs is 1.2×10^{10} microspheres/ml (A. King, 2010). Initially, the vial was left at room temperature for approximately 30 minutes prior to activation. MBs were then activated by using Vial-Mix (Lantheus Medical Imaging, Billerica, MA, USA) for 45-seconds. It was then equilibrated for 5 minutes at the room temperature. The vial was agitated horizontally for 10 seconds by hand. It was then inverted for 30 seconds prior to venting with an 18-gauge needle. The total volume per sample was 1.5 mL. For each sample, 1% volume concentration of Definity® MBs, 15 µL (~1.8×10^8 microspheres), was diluted in 60 µL PBS with 1:4 ratio. The diluted sample was then add into the remaining exposure media of either cells or degassed water.

2.4 USMB EXPERIMENTAL SETUP

The experimental setup is shown in Fig. 2.2. It consists of a water tank, two transducers (a transmit transducer mounted at a 90^0 angle from a passive transducer) attached to a micro-positioning system and a needle phantom to position the foci of the transducers, and a cylindrical chamber (inner diameter of 4 mm) placed at the focal region of the transducers. A 1.0 MHz (IL0208HP, Valpey Fisher Inc., Hopkinton, MA) center frequency transducer (diameter = 42 mm; focal length = 4.8 cm; beamwidth = 2.0 mm) was used for the treatment. A 2.25 MHz (IL0208HP, Valpey Fisher Inc., Hopkinton, MA) center frequency transducer (diameter = 25

mm; focal length = 8 cm; beamwidth = 2.0 mm) was used as a passive transducer to detect MBs' cavitation activity during US insonation.

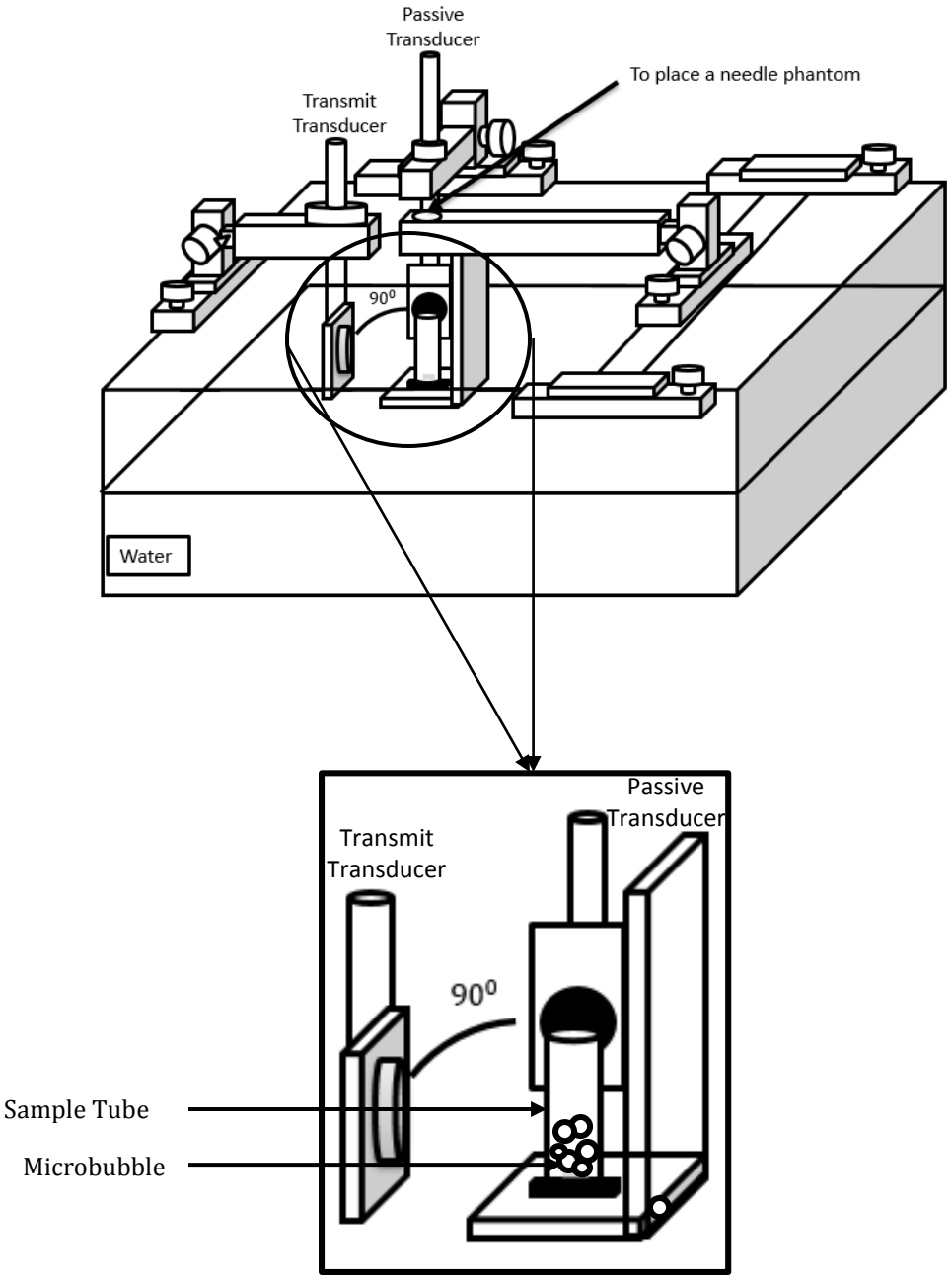

A

B

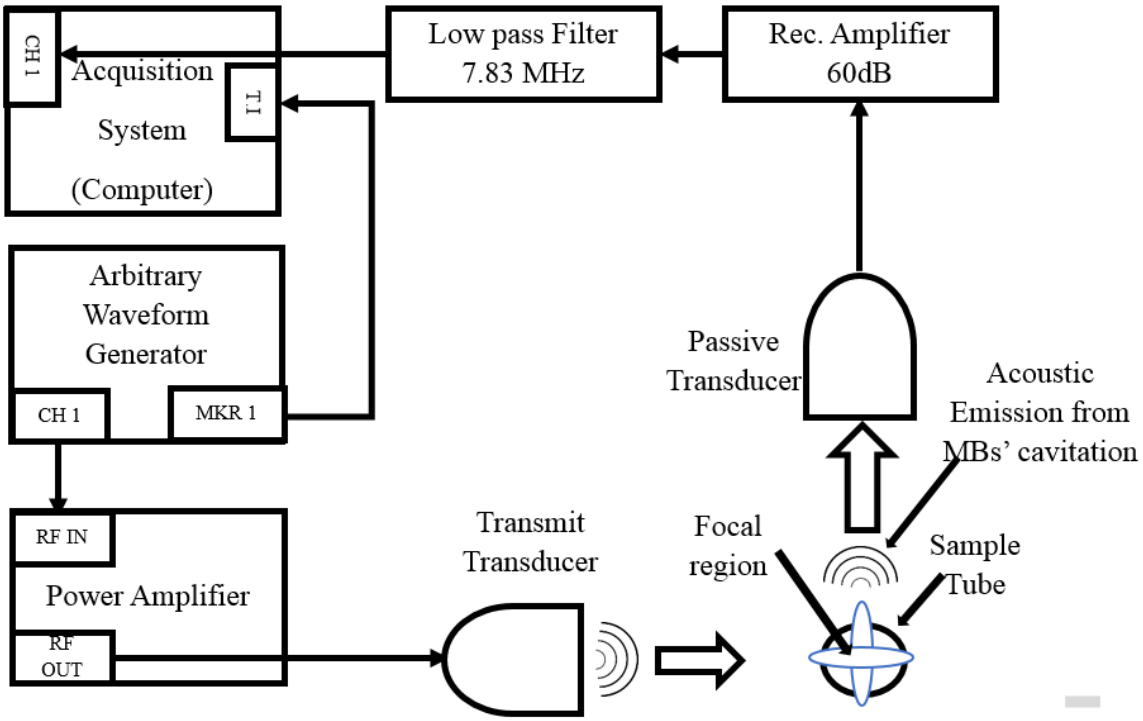

C

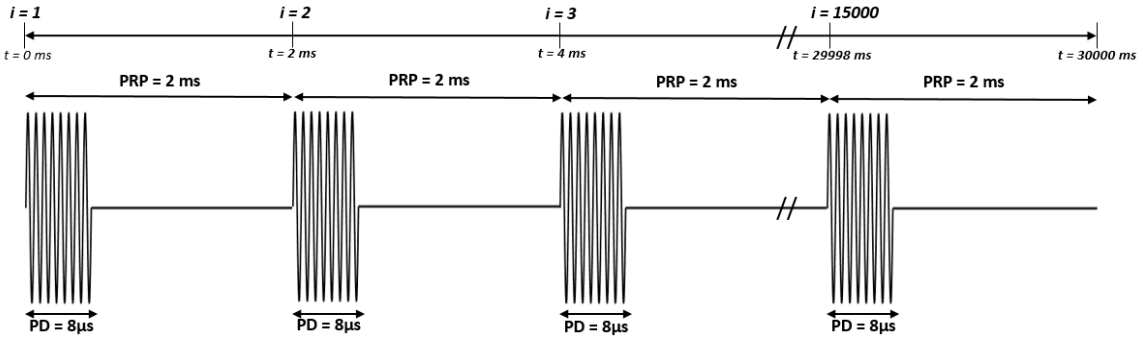

Figure 2.2: (A) schematic diagram of setup with transmit transducer and passive transducer mounted perpendicularly. (B) Block diagram of the top view of the experimental set up shown in A with inclusion of US equipment. (C) A train of ultrasound pulses transmitted by the transmit transducer

A 100Msample/sec arbitrary waveform generator (Sony Tektronix AWG 5002C, Tektronix Japan, Ltd., Tokyo, Japan) was connected to an RF amplifier (Electronics & Innovation, Ltd., Rochester, U.S.A), which was connected to the transmit transducer (Fig. 2.2 B). The receive transducer was connected to a 60dB low noise (RF) amplifier (Miteq, USA), which was connected to the CompuScope MATLAB SDK (CompuScope MATLAB SDK, Lockport, IL, USA) analog to digital (A/D) acquisition system on the computer. The acquired signal was saved on the computer in the form of time domain for post analysis.

Calibration of the transmit transducer

The transmitting transducer was calibrated to determine the amplitude of the waveform at the focal point followed by conversion of amplitudes in voltage to the acoustic pressure in pascal. To calibrate the transmitting transducer, an eight cycle tone bursts with a PRF of 100 Hz at the center frequency of transmitting transducer was generated by using a pulser-receiver setup. A calibrated needle hydrophone with an active element diameter of 400 μm (HNA-0400; Onda corp., Sunnyvale, CA, USA) was positioned at the focal point of the transducer. The strength of acoustic signal at the focal point was recorded in the unit of peak rarefactional voltage, which was then converted in the unit of Pascal. The transducer was calibrated for a range of acoustic waveform amplitudes. The calibration curve is attached in the appendix of this dissertation.

Bandwidth of the passive transducer

The bandwidth of passive transducer was determined by placing a flat glass plate reflector at the focus of the 2.25 MHz passive transducer using pulse echo mode. The signal was acquired on computer via acquisition system. The normalized amplitude spectrum of the passive transducer's bandwidth was used for bandwidth correction. The characteristics of passive

transducer including beamwidth and fractional bandwidth at full width half maximum (FWHM) is shown in appendix of this dissertation.

2.4.1 US exposure conditions

The constant ultrasound parameters were: pulse repetition period (PRP) = 2 ms; pulse duration period (PDP) = 8μs; insonation time = 30 seconds; acoustic frequency = 1.0 MHz. A varying US parameter was peak negative pressures (PNPs), which, at the focal point, were 0.19, 0.37, 0.48, 0.57, 0.64, 0.80, 0.95, 1.12 and 1.26 MPa. The cavitation experiments were performed in the absence and presence of cells, respectively. In the absence of cells, the sample was consisted of water and Definity® MBs. In presence of cells, the sample was consisted of MDA cells, Definity® MBs and a permeability marker.

2.5 ANALYSIS

2.5.1 Data Acquisition

The background signal (y_{BG}) was recorded at each PNP for both, the absence and presence of cells. In the absence of cells, the background sample was consisted of water only. In the presence of cells, the background sample was consisted of cells and media. The normalized FFT of an acoustic signal from the background sample, $\left|\frac{Y_{BG}(f)}{Nc}\right|^2$, was then subtracted from the normalized FFT of an acoustic signal from their corresponding cavitation experiments, $\left|\frac{Y_{CE}(f)}{Nc}\right|^2$. The resulting spectrum after subtraction was denoted as P_R (f) and was corrected for the bandwidth, P_{BW} (f), of the transducer. The final spectrum was denoted as P_{MB} (f) (Fig.2.3) and used for generating power spectrums and further quantification of Integrated Cavitation Dose (ICD).

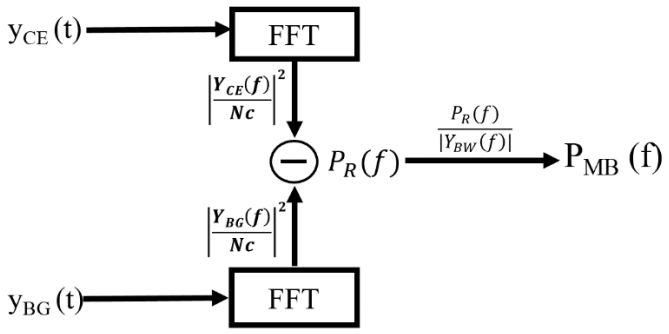

Figure 2.3: A block diagram of spectral subtraction and bandwidth correction.

In figure 2.3,

$y_{CE}(t)$ = Time domain signals from MBs' cavitation experiments

$y_{BG}(t)$ = Time domain signals from the background sample

$\left|\frac{Y_{CE}(f)}{Nc}\right|^2$ = Normalized FFT power spectrum of $y_{CE}(t)$; N_c represents the normalization coefficient, which equals to the length of time domain signal

$\left|\frac{Y_{BG}(f)}{Nc}\right|^2$ = Normalized FFT power spectrum of $y_{BG}(t)$; N_c represents the normalization coefficient, which equals to the length of time domain signal

$P_R(f)$ = The FFT spectrum after spectral subtraction

$Y_{BW}(f)$ = The normalized FFT spectrum of bandwidth of passive transducer

$P_{MB}(f)$ = The final spectrum after spectral subtraction and bandwidth correction

2.5.2 Integrated Cavitation Dose (ICD)

The area under the harmonics ($2f_0$ and $3f_0$) and ultra-harmonics ($\frac{5}{2}f_0$ and $\frac{7}{2}f_0$) of the final spectrum, P_{MB} (f), was used to assess the cavitation activities of MBs (Lai et al., 2006). The area was quantified in a band of Δf = 500 KHz and defined as integrated cavitation dose, $\boldsymbol{ICD_i^{Mf_0}}$, of harmonics ($\boldsymbol{ICD_i^{2f_0}}$ **and** $\boldsymbol{ICD_i^{3f_0}}$) and ultra-harmonics ($\boldsymbol{ICD_i^{\frac{5}{2}f_0}}$ **and** $\boldsymbol{ICD_i^{\frac{7}{2}f_0}}$) for a given pulse **(Eqn. 2.1)**. This was followed by the summation of $ICD_i^{Mf_0}$ over total insonation

time of 30 s for each harmonic and ultra-harmonic where i represents pulse no. from 1 to 15000 and Δt represents PRP **(Eqn. 2.2)**. Table 2.1 summarizes the frequency windows selected for the ICD calculation.

$$ICD_i^{Mf_0} = \sum_{Mf_0-\frac{1}{2}\Delta f}^{Mf_0+\frac{1}{2}\Delta f} P_{MB_i}(f) \qquad \text{[Eqn. 2.1]}$$

$$ICD^{Mf_0} = \sum_{i=1}^{i=\frac{Total\ Time(s)}{PRP(s)}} ICD_i^{Mf_0}\,\Delta t \qquad \text{[Eqn. 2.2]}$$

Table 2.1: ICD regions for frequencies, f, at which MBs generated energy

$\boldsymbol{ICD_i^{Mf_0}}$	$\boldsymbol{Mf_0}$ **[MHz]**	$\boldsymbol{Mf_0 - \frac{1}{2}\Delta f}$ **[MHz]**	$\boldsymbol{Mf_0 + \frac{1}{2}\Delta f}$ **[MHz]**
$ICD_i^{2f_0}$	2.0	1.75	2.25
$ICD_i^{\frac{5}{2}f_0}$	2.5	2.25	2.75
$ICD_i^{3f_0}$	3.0	2.75	3.25
$ICD_i^{\frac{7}{2}f_0}$	3.5	3.25	3.75

The broadband ICD was defined as the summation of the ICD of harmonics and ultra-harmonics **(Eqn. 2.3)**. This was followed by the summation of ICD_i^{BB} over total insonation time of 30 seconds; where i represents pulse no. from 1 to 15000 and Δt represents PRP (**Eqn. 2.4)**.

$$ICD_i^{BB} = ICD_i^{2f_0} + ICD_i^{\frac{5}{2}f_0} + ICD_i^{3f_0} + ICD_i^{\frac{7}{2}f_0} \qquad \text{[Eqn. 2.3]}$$

$$ICD^{BB} = \sum_{i=1}^{i=\frac{Total\ Time(s)}{PRP(s)}} ICD_i^{BB}\,\Delta t \qquad \text{[Eqn. 2.4]}$$

Figure 2.4 shows pictorial presentation of how the broadband ICD was quantified over total insonation time, ICD^{BB}, from the final spectrum, P_{MB} (f).

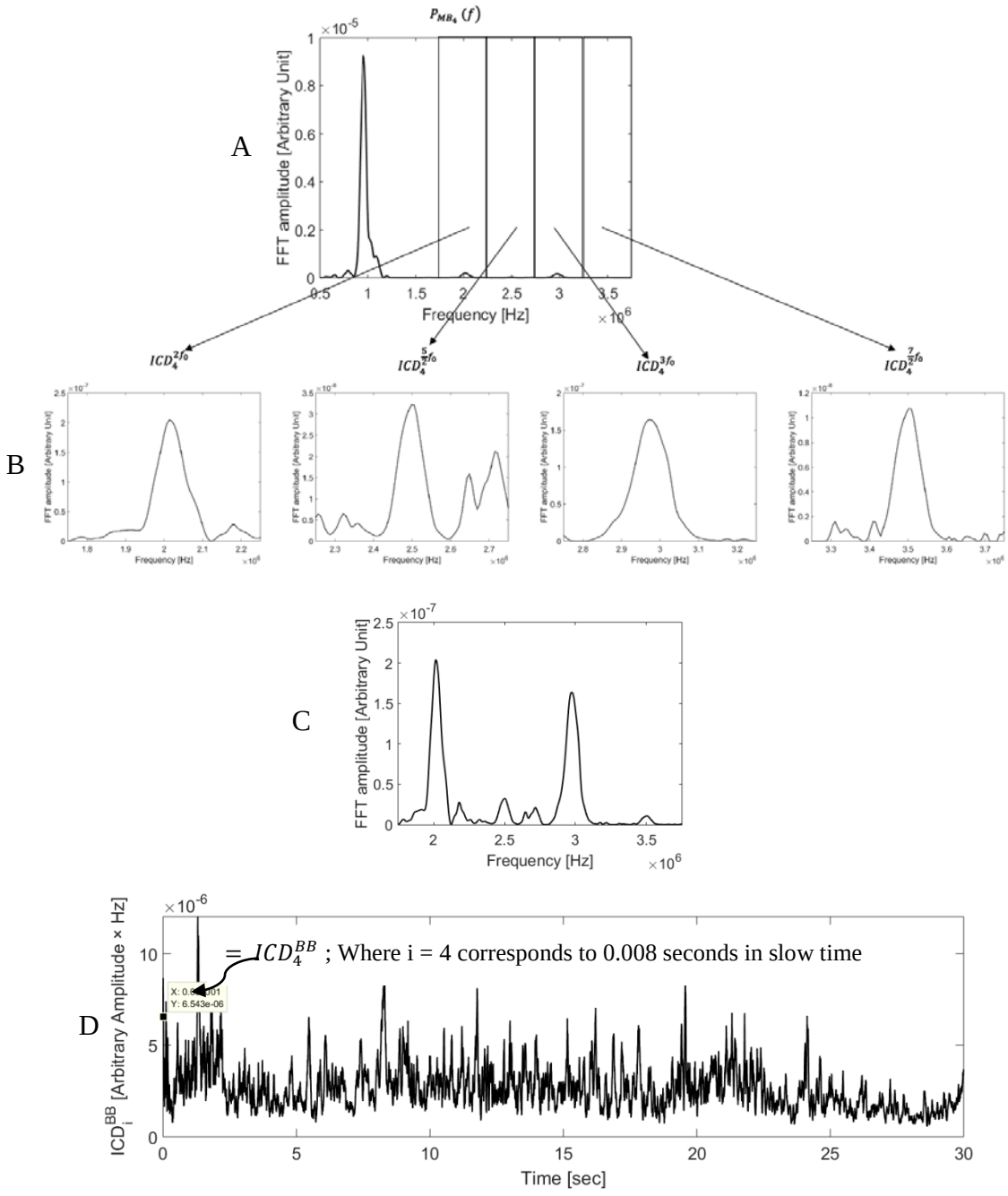

Figure 2.4: The diagrammatic schematic of quantifying the broadband ICD over total insonation time, ICD^{BB} . **A,** The final spectrum, P_{MB_4}; where i corresponds to pulse No. 4. **B,** Zoomed in to 2nd harmonic, 2nd ultra-harmonic, 3rd harmonic and 3rd ultra-harmonic frequency windows for the ICD quantification. **C,** The broadband frequency window from 1.75 MHz to 3.75 MHz, the summation of $ICD_4^{2f_0}$, $ICD_4^{\frac{5}{2}f_0}$, $ICD_i^{3f_0}$ and $ICD_i^{\frac{7}{2}f_0}$. **D,** The summation of broadband ICD for each pulse $i_{1\rightarrow 15000}$ as a function of total insonation time of 30 seconds.

2.5.3 Inertial Cavitation PNP-threshold

Broadband emission is one of the acoustic characteristics of MBs undergoing inertial cavitation (Chomas et al., 2001; A. King et al., 2010). In present study, a PNP threshold of MBs was defined as the smallest PNP that elicited a significant ($P<0.05$) increase in the broadband ICD, ICD^{BB}**.** An independent sample one tailed student's t-test was performed to compare the broadband ICD, ICD^{BB}, between each PNP (Radhakrishnan et al., 2013). It is generally assumed that MBs undergo stable cavitation below the threshold and inertial cavitation above the threshold (Radhakrishnan et al., 2013; Forbes et al., 2011).

CHAPTER 3: RESULTS

This chapter describes the experimental results of MB acoustic response obtained from the PCD setup shown chapter 2. It evaluates the acoustic behavior of Definity® MBs in both the absence and presence of cells with varied PNPs. The experimental results were analyzed using the integrated cavitation dose (ICD) at varying PNPs. The cavitation stage of MBs in both absence and presence of cells was identified based on statistical analysis performed within different PNPs. Section 3.2 discusses the effects of PNPs on the uptake of a fluorescence molecule FITC dextran. Finally, the correlation between the ICDs and the intracellular uptake of FITC dextran (FITC-positive cells) is shown in section 3.3.

3.1 CHARACTERIZATION OF DEFINITY® MBs IN THE ABSENCE AND PRESENCE OF CELLS

MBs' acoustic response in the absence of cells: Effects of PNP

Figure 3.1 depicts the voltage-time signals of a scattered echo, when a suspension of MBs in the absence of cells was exposed to an ultrasonic pulse at a given PNP ranging from 0.19 to 1.12 MPa. The y-axis represents the unit of voltage in which the scattered echo from MBs' suspension was recorded (Fig. 3.1). Figure 3.2 shows the corresponding spectrums depicting spectral energies. The x-axis represents frequency in hertz and y-axis represents the amplitude in decibel (Fig. 3.2). The constant US parameters were: 2ms PRP, 8 cycles tone burst pulse, 1.0 MHz acoustic frequency and 30 seconds total exposure time.

The voltage amplitude of the scattered echo from MBs suspension increased with PNP (Fig. 3.1). The maximum peak positive voltage value of the scattered signal increased from 0.016 V to 1.451 V as PNP increased from 0.19 MPa to 1.12 MPa (Fig. 3.1 A – H). Moreover, the

scattered signals from MBs were asymmetric, where the value of peak positive voltage is different from that of peak negative voltage (Fig. 3.1), which becomes more evident at PNPs above 0.64 MPa. In addition, at 0.19 MPa, MBs only emitted the fundamental harmonic and second harmonic energy (Fig. 3.2 A). As PNP increased from 0.37 to 0.57 MPa, the second harmonic, second ultra-harmonic and third harmonic amplitudes increased from -128.9 dB to -98.32 dB, from -216.3 dB to -177.0 and from -192.5 dB to -188.2 dB respectively (Fig. 3.2 B – D). As PNP increased from 0.57 to 0.64 MPa, MBs emitted a broadband spectrum with a rapid increase in second ultra-harmonic and third harmonic amplitudes from -177 dB to -122.3 dB and -188.2 dB to -166.8 dB, respectively (Fig. 3.2 D and E). With further increase in PNP to 0.8 MPa, the second ultra-harmonic and third harmonic amplitudes further increased to -45 dB and -146.9 dB, respectively (Fig. 3.2 E and F). MBs generated an intense broadband spectrum at 0.95 and 1.12 MPa with further increase in harmonics and ultra-harmonics amplitudes (Fig. 3.2 G – H).

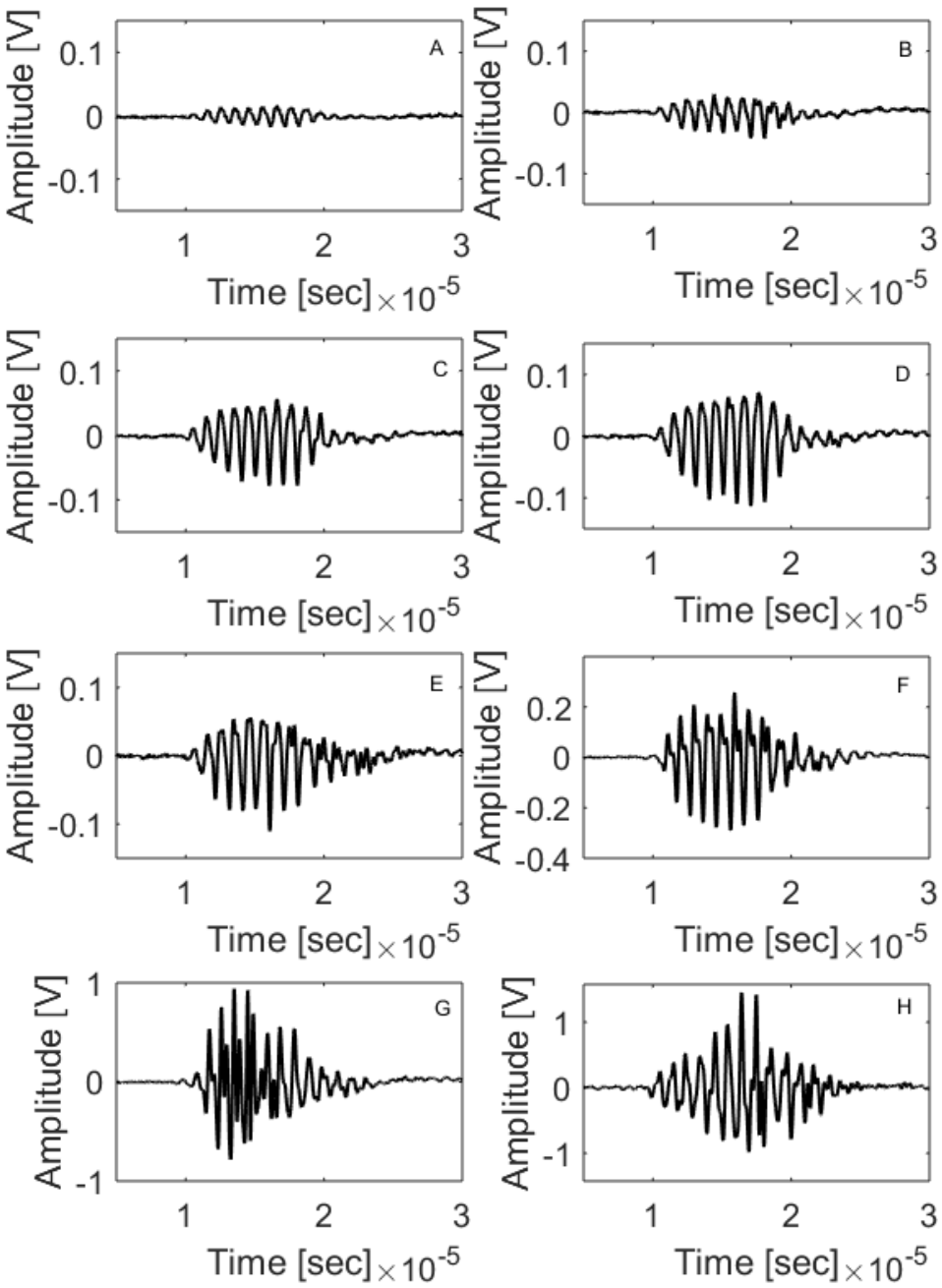

Figure 3.1: Scattered echoes (Voltage-Time signals) from Definity® in the absence of cells at different peak negative pressures (PNPs): (A) 0.19 MPa; (B) 0.37 MPa; (C) 0.47 MPa; (D) 0.57 MPa; (E) 0.64 MPa; (F) 0.8 MPa; (G) 0.95 MPa and (H) 1.12 MPa

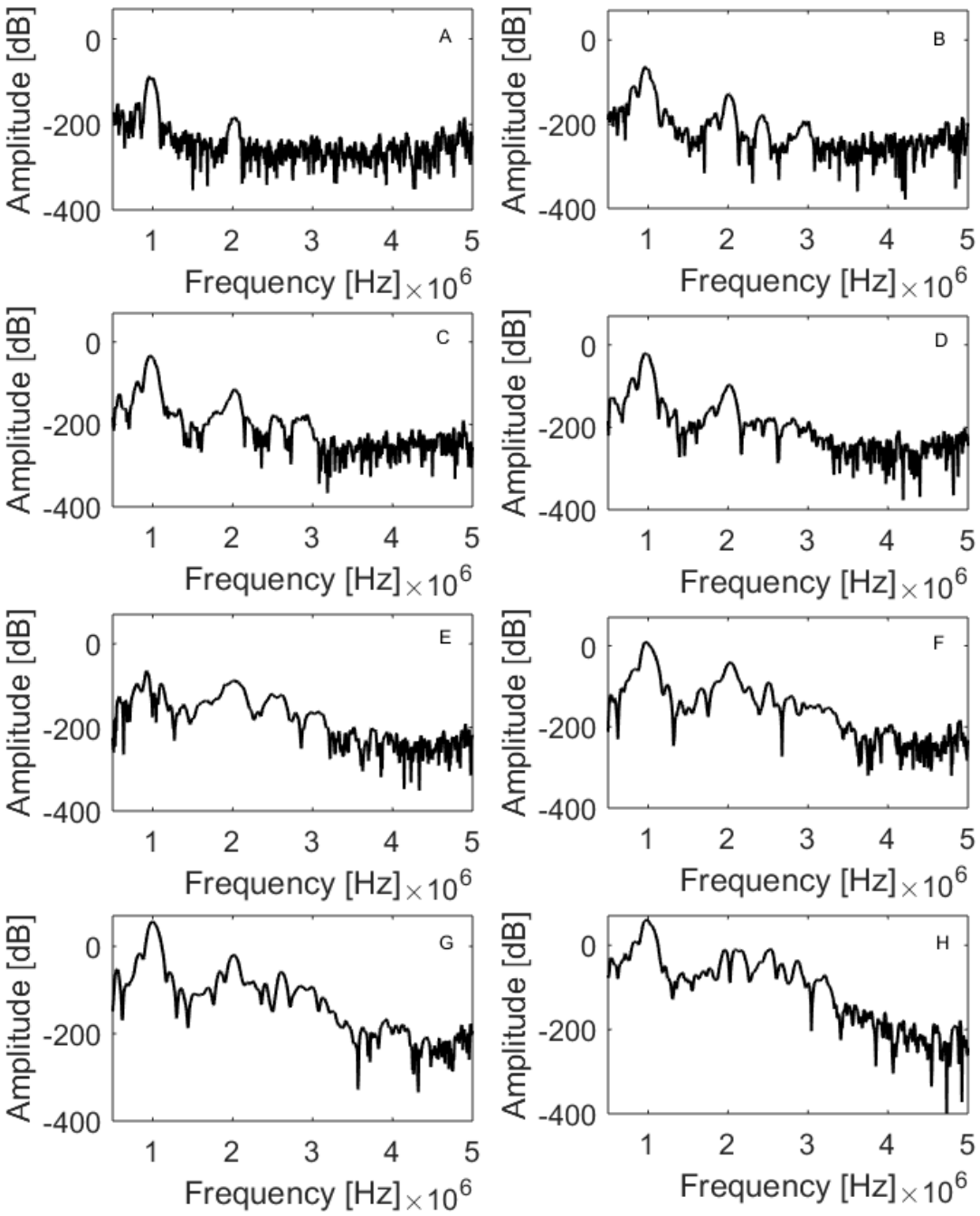

Figure 3.2: Spectral energies generated by Definity® in the absence of cells at different peak negative pressures (PNPs): (A) 0.19 MPa; (B) 0.37 MPa; (C) 0.47 MPa; (D) 0.57 MPa; (E) 0.64 MPa; (F) 0.80 MPa; (G) 0.95 MPa and (H) 1.12 MPa.

MBs' acoustic response in the presence of cells: Effects of PNP

Figure 3.3 depicts the voltage-time signals of a scattered echo, when a suspension of MBs in the presence of cells was exposed to an ultrasonic pulse with a given PNP ranging from 0.19 MPa to 1.12 MPa (Fig. 3.3). Figure 3.4 shows their corresponding spectrums, where the x-axis represents frequency in Hertz and y-axis represents the intensity amplitude in decibel (Fig. 3.4). The constant US parameters were: 2ms PRP, 8 cycles tone burst pulse, 1.0 MHz acoustic frequency and 30 seconds total exposure time.

The voltage amplitude of the scattered echo from MBs increased with PNP (Fig. 3.3). The maximum peak positive voltage of the scattered signal increased from 0.011 V to 1.104 V as PNP increased from 0.19 MPa to 1.12 MPa (Fig. 3.3 A – H). The asymmetry of scattered signals became more evident at PNPs above 0.64 MPa (Fig. 3.3 E – H). In addition, at 0.19 MPa, MBs emitted the fundamental and second harmonic energy (Fig. 3.4 A). MBs emitted second harmonic, second ultra-harmonic and third harmonic energy between 0.37 and 0.57 MPa (Fig. 3.4 B – D). As PNP increased from 0.57 to 0.64 MPa, MBs generated a broadband spectrum with a rapid increase in second ultra-harmonic from -226 dB to -122.3 dB (Fig. 3.4 D – E). At 0.64 MPa, MBs also exhibited third ultra-harmonic energy (Fig. 3.4 E). MBs generated an intense broadband spectrum at 0.95 and 1.12 MPa with further increase in harmonics and ultra-harmonics amplitudes (Fig. 3.4 G – H). Thus, the amplitude of the scattered echo at 0.19 MPa and 1.12 MPa was comparable in both the absence and presence of cells. Furthermore, the asymmetry of the scattered echoes became more evident at PNPs above 0.64 MPa in both the absence and presence of cells. Moreover, in both the absence and presence of cells, MBs emitted broadband spectrum at higher PNPs (PNP $\geq$ 0.64 MPa) with a comparable harmonics and ultra-

harmonics amplitudes. Thus, the spectral characteristics of MBs at each PNP was similar in both the presence and absence of cells.

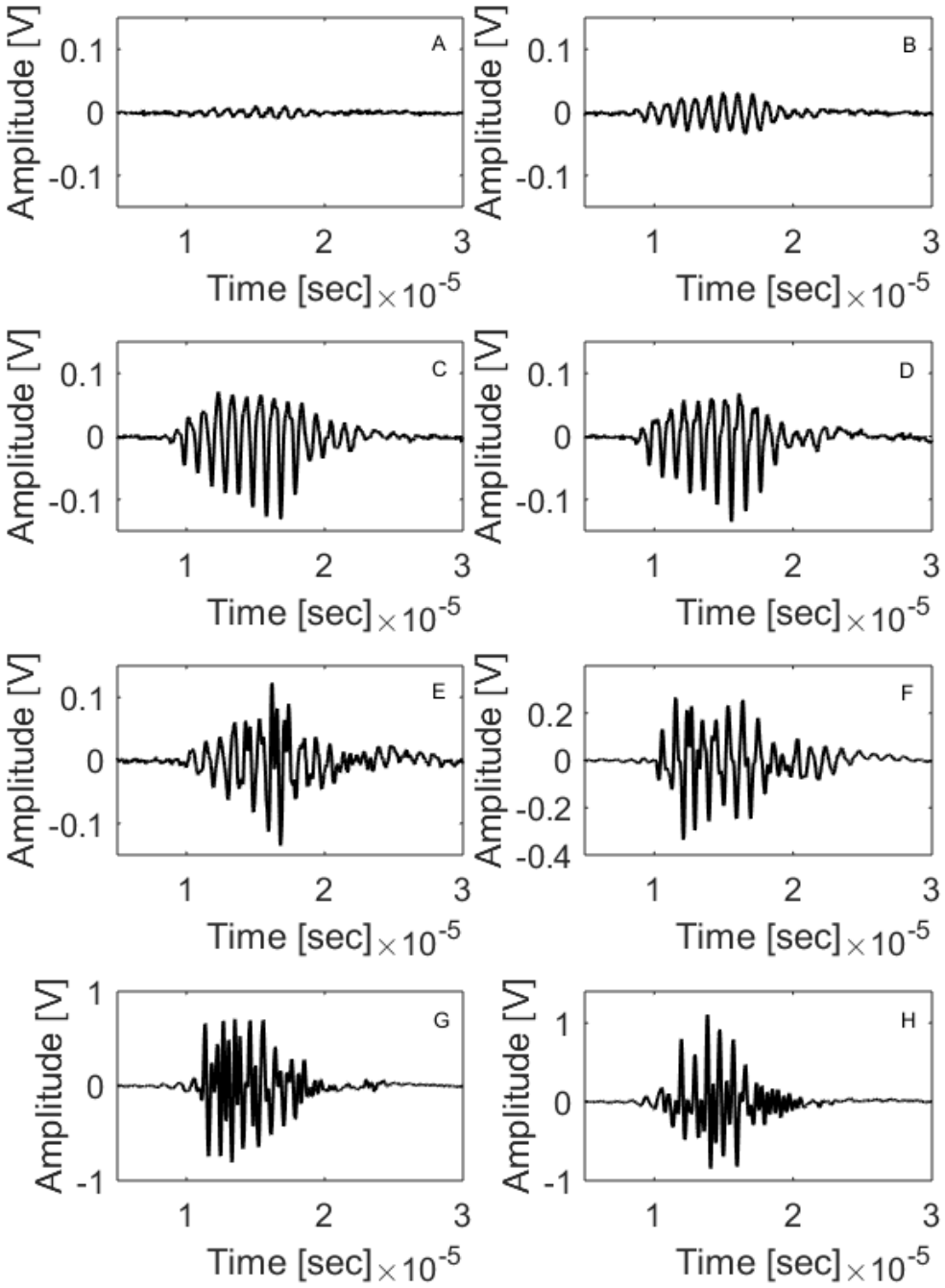

Figure 3.3: Scattered echoes (Voltage-Time signals) from Definity® in the presence of cells at (A) 0.19 MPa; (B) 0.37 MPa; (C) 0.47 MPa; (D) 0.57 MPa; (E) 0.64 MPa; (F) 0.8 MPa; (G) 0.95 MPa and (H) 1.12 Mpa.

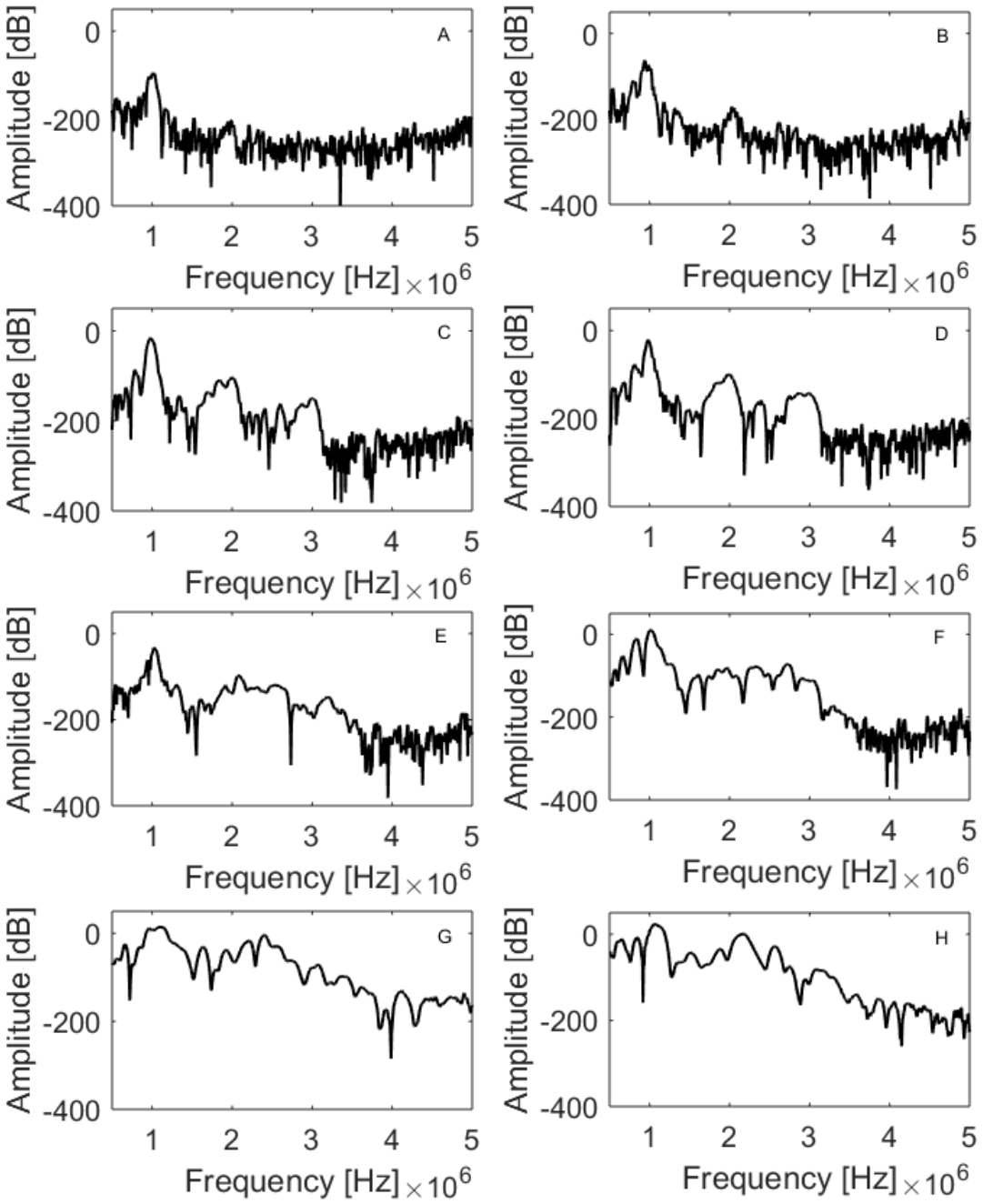

Figure 3.4: Spectral energies generated by Definity® at different peak negative pressures (PNPs): (A) 0.19 MPa; (B) 0.37 MPa; (C) 0.47 MPa, (D) 0.57 MPa; (E) 0.64 MPa; (F) 0.80 MPa; (G) 0.95 MPa and (H), 1.12 MPa in the presence of cells.

Figure 3.5 and 3.6 illustrate the broadband ICD amplitude as a function of exposure time, ICD_i^{BB} (where i represents the number of pulse from 1 to 15000, with pulse repetition period (PRP) of 2 ms to have a total exposure time of 30 seconds), at each PNP in both the absence and presence of cells, respectively. These plots were generated by the procedure delineated in section 2.5.2 (Fig 2.4) and provide an estimation of MBs cavitation activities at each PNP during US exposure.

At 0.19 MPa, the ICD amplitude remains steady throughout the entire exposure time in both the absence and presence of cells with a comparable order of magnitude of the ICD amplitude (Fig 3.5A and Fig 3.6A). At PNPs between 0.37 and 0.57 MPa, the order of magnitude of the ICD amplitude was also comparable, 10^{-6}, in both the absence and presence of cells.

At 0.64 MPa, however, the order of magnitude of the ICD amplitude increased by a factor of 10 in both the absence and presence of cells (Fig 3.5 E and Fig 3.6 E). With further increase in PNP, the ICD amplitude continues to increase in both the absence and presence of cells (Fig 3.5 E and H; Fig 3.6E and H). Thus, the cavitation activities of MBs as a function of exposure time also appeared to be following a similar trend in both the absence and presence of cells, respectively.

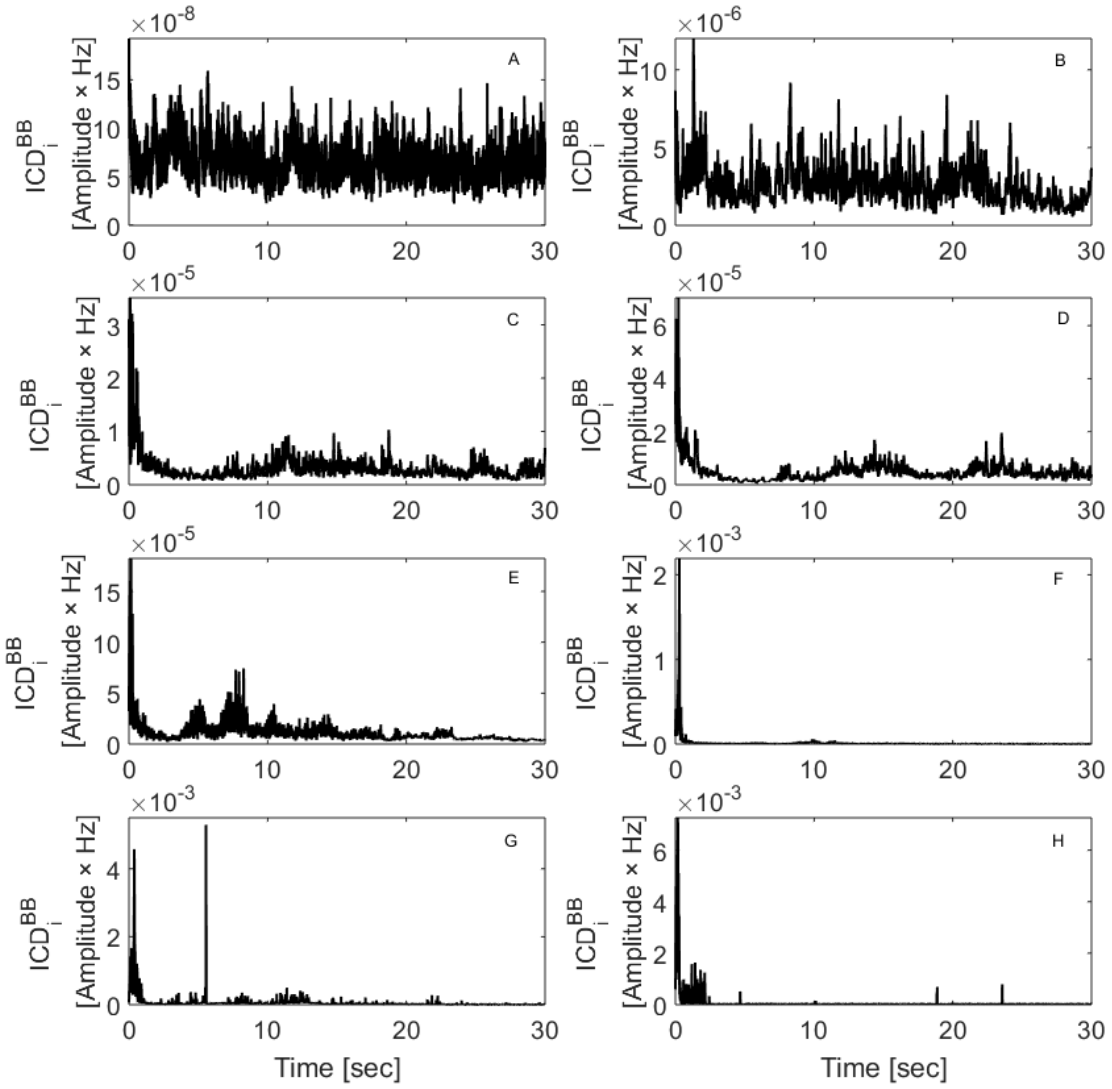

Figure 3.5: Broadband (1.75 – 3.75 MHz) ICD amplitude as a function of total exposure time in the absence of cells at different peak negative pressures (PNPs): (A) 0.19 MPa; (B) 0.37 MPa; (C) 0.47 MPa, (D) 0.57 MPa; (E) 0.64 MPa; (F) 0.80 MPa; (G) 0.95 MPa and (H) 1.12 MPa.

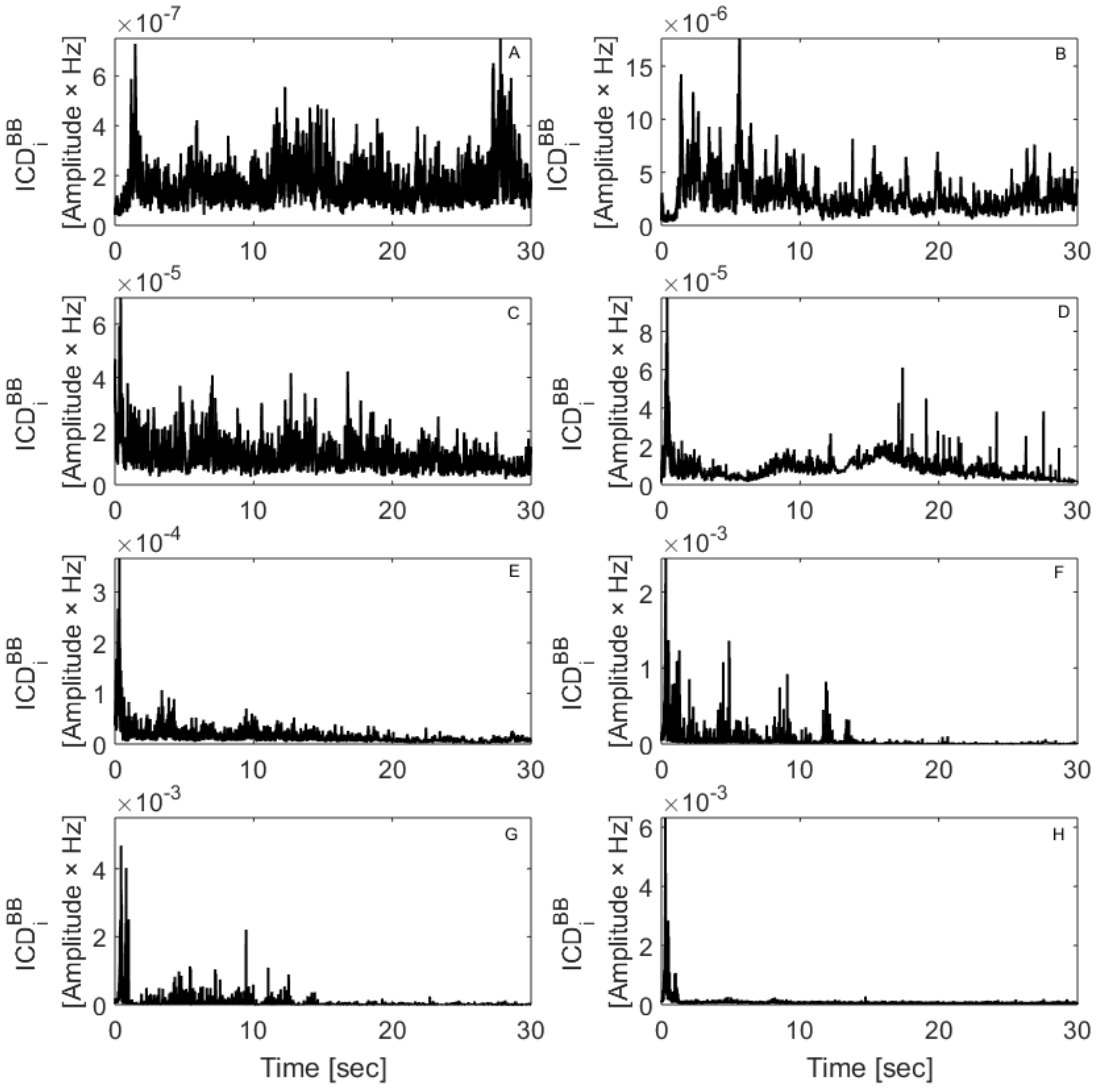

Figure 3.6: Broadband (1.75 – 3.75 MHz) ICD amplitude as a function of total exposure time in the presence of cells at different peak negative pressures (PNPs): (A) 0.19 MPa; (B) 0.37 MPa; (C) 0.47 MPa; (D) 0.57 MPa; (E) 0.64 MPa; (F) 0.80 MPa; (G) 0.95 MPa and (H) 1.12 MPa.

ICD over a range of frequencies in the absence and presence of cells

Figure 3.7 shows the broadband ICD (ICD_{BB}) as a function of PNPs in both the absence and presence of cells. Each point represents the mean and standard deviation for five to eight independent trials. There was no significant difference in the mean value of broadband ICD between 0.37 and 0.57 MPa ($P>0.05$). As PNP increased from 0.57 to 0.64 MPa, a significant increase in the mean value of the ICD was observed ($P<0.05$). With further increase in the PNP, the mean value of the ICD continued to increase significantly ($P<0.05$). Thus, based on an independent sample one tailed t-test, the PNP threshold at which MBs undergo inertial cavitation was observed to be 0.64 MPa (Fig 3.7). Thus, the PNPs regimes for stable and inertial cavitation of MBs were observed to be PNPs<0.64 MPa and PNP≥0.64 MPa, respectively.

Below the threshold (PNP<0.64MPa), the mean broadband ICD values are comparable in the presence and absence of cells. Whereas, above the threshold, the mean broadband ICD values in the presence of cells are greater than those in the absence of cells. However, the difference is not statistically significant as the mean broadband ICD values in the absence of cells were within the standard deviation of the ones in the presence of cells (Fig 3.7). Similar trend was observed for second ultra-harmonic and third ultra-harmonic ICD values at PNPs below and above the threshold, respectively (Fig 3.8).

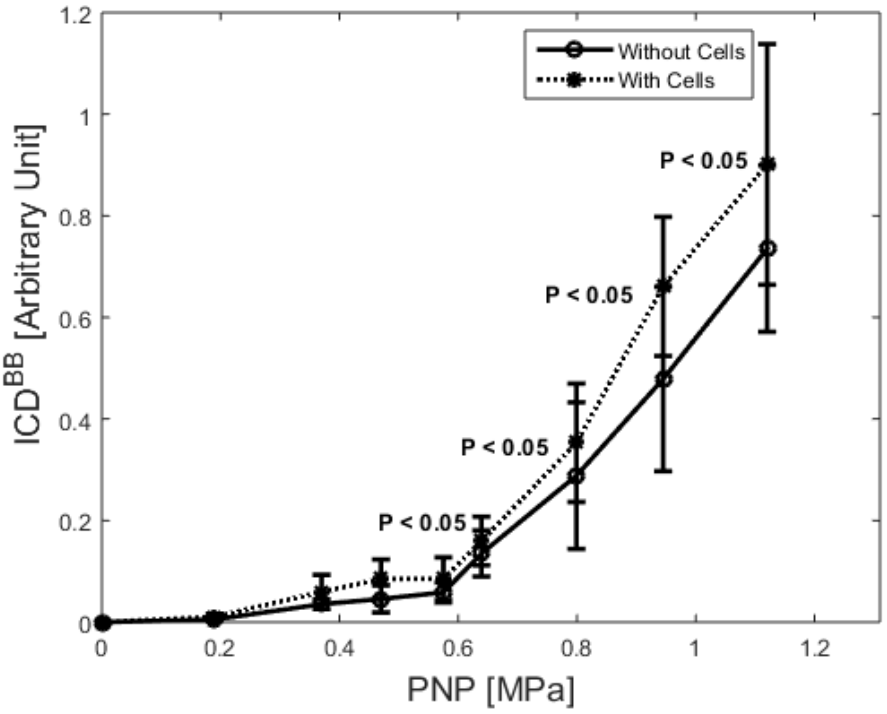

Figure 3.7: The broadband ICD, ICD^{BB}, as a function of PNP in the presence (dashed line) and absence of cells (solid line). Acoustic frequency = 1.0 MHz, Pulse Duration Period = 8 Cycles, PRP = 2ms, Total Exposure time = 30 s.

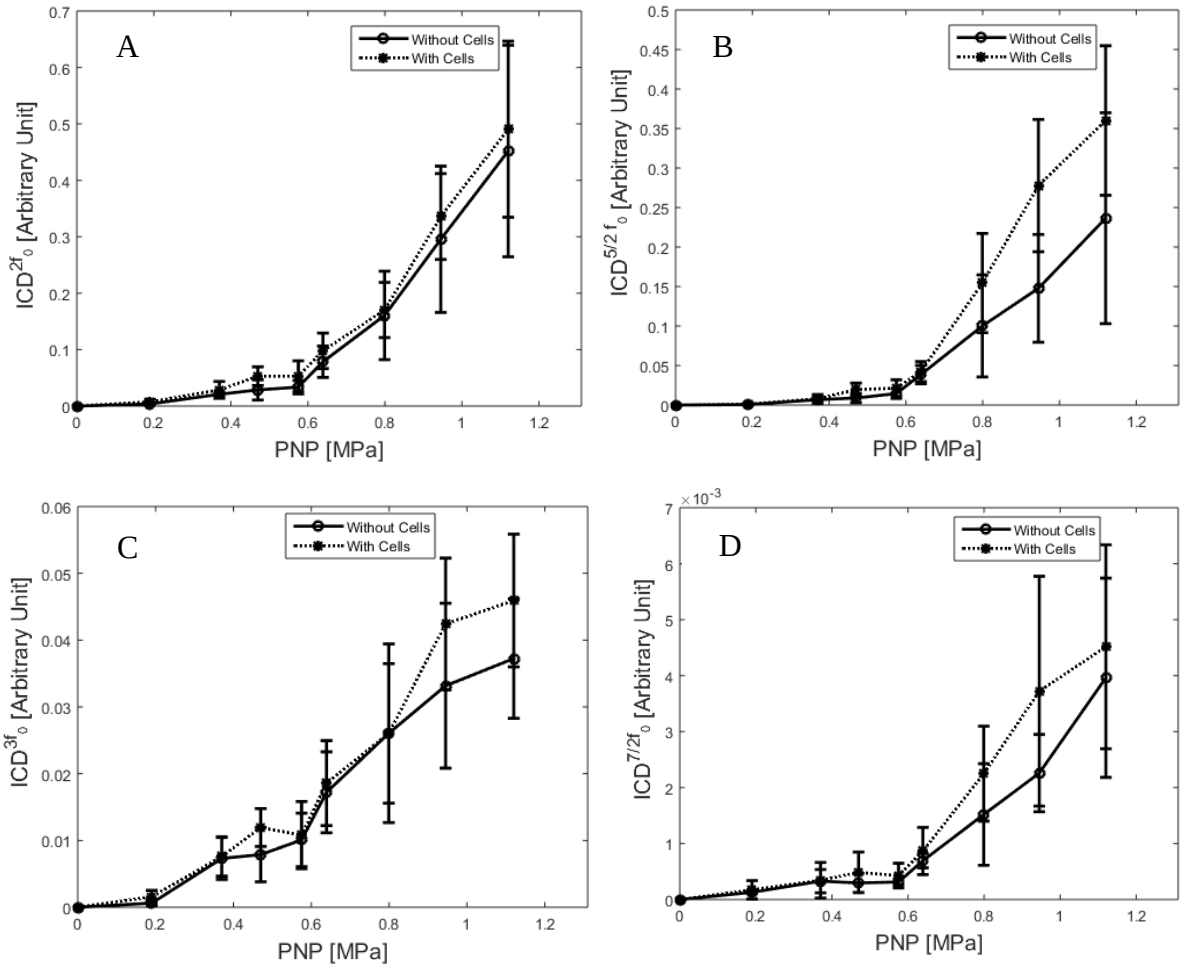

Figure 3.8: Comparison of (A) second harmonic, (B) second ultra-harmonic, (C) third harmonic and (D) third ultra-harmonic ICD in the absence of cells (solid line) and in the presence of cells (dashed line) Acoustic frequency = 1.0 MHz, Pulse Duration Period = 8 Cycles, PRP = 2ms, Total Exposure time = 30 s.

3.2 EFFECTS OF PNP ON THE INTRACELLULAR UPTAKE

The intracellular uptake of a cell permeability marker, FITC-Dextran, was measured at PNPs ranging from 0.19 MPa to 1.26 MPa, which spans both stable and inertial cavitation regimes of MBs. Figure 3.9 shows the percentage of FITC positive cells (intracellular uptake) as a function of PNPs. Each point represents the mean and standard deviation for five to eight independent trials. At 0.19 MPa, the percentage of FITC positive cells is below one percent. The percentage of FITC positive cells increased from 0.89% ± 0.16% to 5.94% ± 1.03% as PNP increased by 390 kPa, from 0.19 MPa to 0.57 MPa. Whereas, as PNP increased from 0.57 MPa to 0.64 MPa, there appeared to be a sudden increase in the percentage of FITC positive cells from 5.94% ± 1.03% to 13.13% ± 2.70% (Fig 3.9). With a further increase in PNPs above 0.64 MPa, the percentage of FITC positive cells increased up to 39.93% ± 6.93% (Fig 3.9 A). The percentage of FITC pos. cell increased at a higher rate (~ 3.3 fold) within inertial cavitation regime compared to stable cavitation regime (Fig 3.9 B). A strong correlation ($R^2 > 0.9$) was observed within both stable and inertial cavitation regime (Fig 3.9 B).

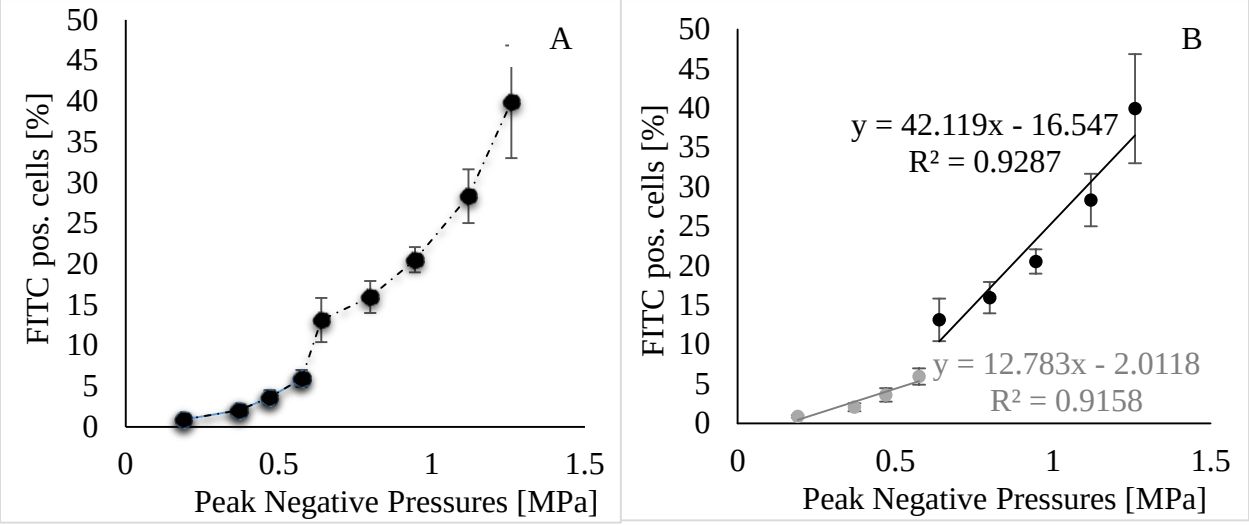

Figure 3.9: Effects of PNP on the percentage of FITC positive cells exposed to USMB at PD = 8 µs; PRP = 2ms; frequency = 1 MHz; insonation time = 30 seconds: (A) Without considering

MBs' cavitation regime, (B) With considering MBs' stable cavitation regime (grey circles) and the inertial cavitation regime (black circles).

3.3 CORRELATION BETWEEN THE ICD OVER A RANGE OF FREQUENCIES AND INTRACELLULAR UPTAKE

In the previous two sections, we characterized the acoustic behavior of MBs at varying PNPs by quantifying the ICD. From acoustic characterization of MBs, we observed a wide range of MBs' cavitation dynamics from stable cavitation (PNP < 0.64 MPa) to inertial cavitation (PNP ≥ 0.64 MPa). In this section, the correlation between the ICD over a range of frequencies and the percentage of FITC-positive cells (intracellular uptake) was assessed with (Fig. 3.10 B and Fig. 3.11 E – H) and without (Fig. 3.10 A and Fig. 3.11 A – D) considering MBs' stable and inertial cavitation regime. In figure 3.10 B and 3.11 E – H, the grey circles represents stable cavitation regime, whereas black circles represents inertial cavitation regime. Each point represents the mean and standard deviation for five to eight independent trials.

When MBs' cavitation regimes are not considered, the percentage of FITC positive cells appeared to be strongly correlated with the ICD quantified over broadband (R^2=0.96), 2nd harmonic (R^2=0.95), 2nd ultra-harmonics (R^2=0.95), 3rd harmonic (R^2=0.97) and 3rd ultra-harmonic (R^2=0.95), respectively (Fig. 3.10 A and Fig. 3.11 A – D).

In inertial cavitation regime, the percentage of FITC positive cells appeared to be strongly correlated (R^2 > 0.9) with the ICD for broadband (Fig 3.10 B), harmonics and ultra-harmonics (Fig. 3.11 E – H); the strongest correlation appeared to be between FITC positive cells and the broadband ICD (R^2 = 0.98). In stable cavitation regime, the correlation appeared to be weaker for 3rd harmonic (R^2 = 0.64) and 3rd ultra-harmonic (R^2 = 0.59). Nonetheless, the

correlation was $R^2 = 0.71$, $R^2 = 0.78$, $R^2 = 0.85$ for broadband (Fig. 3.10 B), 2nd harmonic (Fig. 3.11 E) and 2nd ultra-harmonic (Fig. 3.11 F), respectively.

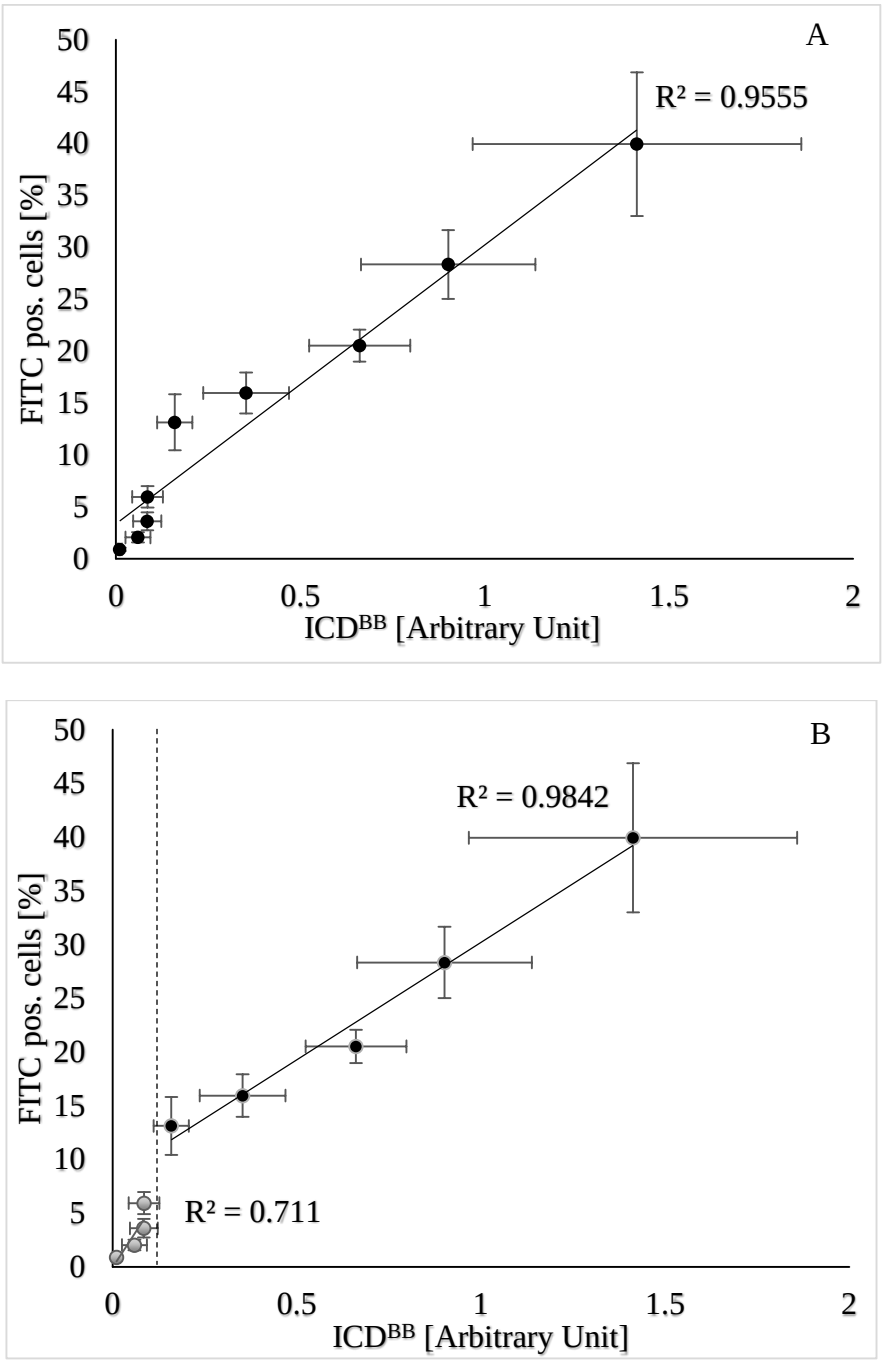

Figure 3.10: Correlation between the broadband ICD and the percentage of FITC positive cells: (A) Without considering MBs' cavitation regime, (B) With considering MBs' stable cavitation regime (grey circles) and the inertial cavitation regime (black circles).

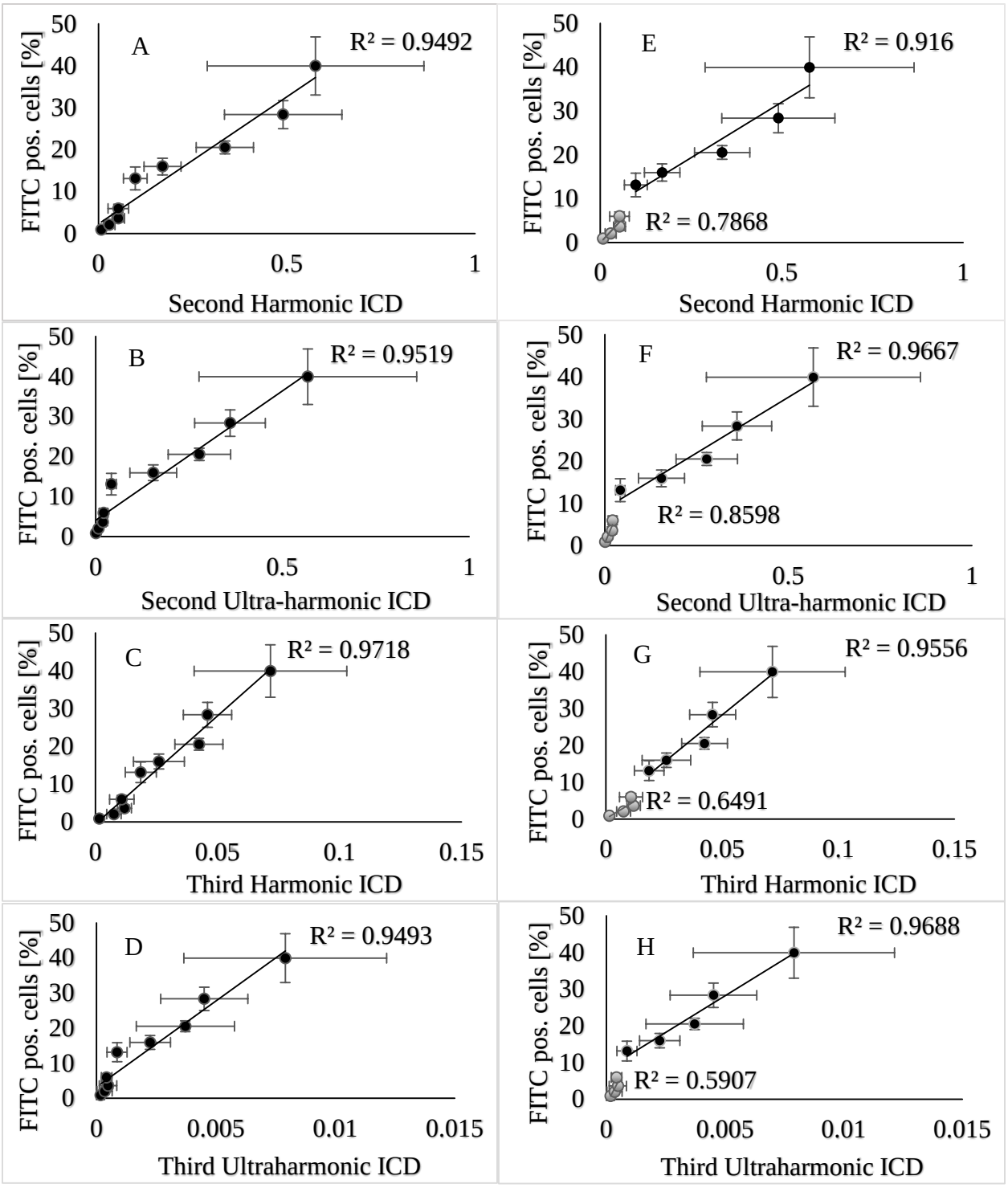

Figure 3.11: Correlation between the 2nd harmonic, 2nd ultra-harmonic, 3rd harmonic and 3rd ultra-harmonic ICDs and the percentage of FITC positive cells: **(A – D)** Without considering MBs' cavitation regime, **(E – H)** With considering MBs' stable cavitation regime (grey circles) and the inertial cavitation regime (black circles).

CHAPTER 4: DISCUSSIONS AND CONCLUSIONS

4.1 MB ACOUSTIC BEHAVIOR IN THE ABSENCE AND PRESENCE OF CELLS

The present study characterized the acoustic behavior of Definity® MBs at varied PNPs and identified the PNP-threshold using broadband emission (ICD^{BB}) as an indicator of MB inertial cavitation (De Jong et al., 2009; Chen et al., 2003). In general, it is assumed that most MBs undergo stable cavitation at PNPs below the PNP-threshold, whereas, at PNPs above the PNP-threshold, most MBs undergo inertial cavitation (Radhakrishnan et al., 2013; Forbes, 2011). The PNP threshold at which MBs in the sample undergo inertial cavitation appeared to be 0.64 MPa, which is comparable to another study on Definity® MBs (King D.A. et al., 2010). Whereas a higher PNP threshold was found in studies on Definity® MBs, with pulse duration period (PDP) of 5 μs (Forbes et al., 2011; Haak et al., 2007) compared to 8 μs in this study. For lipid shelled MBs, it has been shown that the PNP-threshold for inertial cavitation of MBs decreases with increasing pulse duration period (PDP), which increases the acoustic energy delivered to microbubbles (Guo et al., 2013).

Our results showed that the ICD increases with PNP, which is in agreement with earlier studies (Qiu et al., 2010; Lai et al., 2006; Hwang et al., 2006). The broadband ICD increased more rapidly with PNP above the PNP-threshold (inertial cavitation regime) compared to below the PNP-threshold (stable cavitation regime). In a previous study, under similar US exposure condition for Optison® MBs (PDP = 20 μs; acoustic frequency = 1.15 MHz; total treatment time = 30 s; PRP = 2 ms), the broadband ICD increased significantly with PNP above the threshold (PNPs > 0.5 MPa) (Chen et al., 2003). In addition, under stable cavitation regime, MBs emit

harmonic and ultra-harmonic frequency components, whose amplitude increases gradually with PNP (Vignon et al., 2013; A. King et al., 2010), which was observed in this study (Fig. 3.2 A – D and 3.4 A – D) within the stable cavitation regime (PNPs<0.64). Whereas, under inertial cavitation regime, MBs emit broadband emission with a rapid increase in the harmonics/ultra-harmonics amplitudes (King D.A. et al., 2010; Sboros, 2008), as observed in the present study (Fig. 3.2 E – F and 3.4 E – F) within inertial cavitation regime (PNPs≥0.64). Above the PNP-threshold, MBs undergoing inertial cavitation can generate free gas bubbles, which can also cavitate and contribute to the scattered emission (De Jong et al., 2009).

Similar ICDs were observed in the presence and absence of cells both within the stable and inertial cavitation regimes. However, on average, higher ICDs were observed within inertial cavitation regime. This may be due to a longer persistence of MBs' cavitation activities within the solution in the presence of cells compared to the absence of cells as observed experimentally: Figure 3.5 E-F (the absence of cells) versus Figure 3.6 E-H (the presence of cells). This study, thus, indicates that the presence of cells may not have a significant influence on MBs' acoustic response at the therapeutic conditions used in this study.

4.2 INTRACELLULAR UPTAKE AT VARYING PNPs

The intracellular uptake of FITC-dextran (FITC positive cells) increased with increasing PNP, which is in agreement with earlier studies on sonoporation (De Cock et al., 2015; Karshafian et al., 2009). However, the uptake increased at a higher rate within inertial cavitation regime compared to stable cavitation regime. The stable cavitation of MBs create microstreaming effects, inducing shear stress on the cell membrane (Lentacker et al., 2014). This biophysical effect stimulates endocytosis, which, although increases with PNP, has been shown to be the main mechanism of FITC-dextran under stable cavitation regime (Lentacker et al.,

2014; De Cock et al., 2015). Inertial cavitation of MBs, on the other hand, generates shock waves and liquid jets in the surrounding media, which generates a very high mechanical stress on the cell membrane. This biophysical effect, in addition to promoting endocytosis, can create membrane pores (Fan et al., 2014). The number and the size these membrane pores increases with PNP, allowing more FITC-dextran molecules to enter the cells (Fan et al., 2014, De Cock et al., 2015). This could cause an increase in the intracellular uptake of FITC-dextran at a higher rate within the inertial cavitation regime compared to stable cavitation regime.

The maximum increase in the intracellular uptake of FITC-dextran (FITC positive cells), with respect to an increase in PNP, occurred at the PNP-threshold. This is presumably due to transition of MBs from stable to inertial cavitation, creating aforementioned biophysical effects in the surrounding environment, which is unlikely to be created by stable cavitation of MBs. Such an increase in bio-effects with the transition in MBs behavior from stable to inertial cavitation has been previously observed (Graham et al., 2014; Tung et al., 2011; Coussios et al., 2008). The blood brain barrier (BBB) opening volume increased from 4% at 0.30 MPa to 20% at 0.45 MPa; the ICD increased significantly ($P<0.05$) as PNP increased from 0.30 MPa to a PNP-threshold, 0.45 MPa (Tung et al., 2011). Furthermore, the percentage of release of luciferin payload from the liposomes increased from 0% to 30% as PNP increased from 0.8 MPa (a PNP identified to be within the stable cavitation regime) to 1.2 MPa (a PNP identified to be within the inertial cavitation regime) (Graham et al., 2014). In a HIFU study, a 9% increase in PNP elevated the temperature of a tissue mimicking phantom by 330%, which was caused by the transition of MBs from stable to inertial cavitation (Coussios et al., 2008). Although our results, to some extent, showed intracellular uptake of FITC positive cells (6.0% ± 1.02%) under stable cavitation

regime, a significant uptake of FITC-dextran (39.94% ± 6.92%) occurred within inertial cavitation regime.

4.3 CORRELATION BETWEEN THE ICD AND INTRACELLUAR UPTAKE

In the present study, the correlation between the intracellular uptake of FITC-dextran and the ICD was assessed with and without considering MBs cavitation regimes with respect to 2^{nd} harmonic, 2^{nd} ultra-harmonic, 3^{rd} harmonic, 3^{rd} ultra-harmonic and broadband spectrum.

This study showed that the correlation between the ICD and intracellular uptake of a cell impermeable molecule depends on the MBs cavitation regime. A strong correlation (R^2>0.9) was found within the inertial cavitation regime irrespective of any harmonic/ultraharmonic/broadband frequencies. Previously, a linear correlation of $R^2 = 0.85$ was observed between the ICD and the blood-brain-barrier opening volume within the inertial cavitation regime (Tung et al., 2011). In contrast, the correlation was weaker within stable cavitation regime ranging from $R^2 = 0.59$ at 3^{rd} ultra-harmonic to $R^2 = 0.85$ at 2^{nd} ultra-harmonic. To our best knowledge, the correlation between the ICD and USMB induced bio-effects has not been well addressed for MBs' stable cavitation regime. However, recently, it has been shown that a correlation of $R^2 = 0.82$ was observed for K_{trans} (coefficient for pharmacokinetics of the MR tracer through the opened BBB) within the stable cavitation regime (Sun et al., 2015).The dependence of correlation on MBs' cavitation regime is presumably due to complex cavitation dynamics of MBs, which still requires better understanding for eliciting therapeutic benefits.

Furthermore, without considering MBs cavitation regimes, a strong correlation (R^2>0.9) was found, which is in agreement with the correlation reported in the literature between the ICD of Optison® MBs and hemolysis with $R^2 = 0.9$ (Chen et al., 2003), Levovist® MBs and

sonoporation rate with $R^2 = 0.75$ (Lai et al., 2006), SonoVue® MBs and DNA transfection with $R^2 = 0.9$ (Qiu et al., 2010).

Overall, our results revealed that the efficacy of USMB-induced intracellular uptake is higher within inertial cavitation regime and strongly correlated with the ICD irrespective of harmonics/ultra-harmonics/broadband suggesting that the ICD has a potential to be a predictor of USMB-mediated targeted drug delivery. In general, however, stable oscillation of MBs is more preferable for USMB mediated drug delivery as inertial cavitation poses a very high risk of mechanical damage (Kang et al., 2014). For such applications, the ICD quantified over 2^{nd} ultra-harmonic may still be utilized to potentially predict the bio-effects induced by stable cavitation of MBs.

4.4 CONCLUSIONS, FUTURE WORK AND LIMITATION

The acoustic behaviour of Definity® MBs was characterized in the absence and presence of cells at varying peak negative pressures (PNPs) using passive cavitation detection (PCD). Cavitation activities of MBs were quantified via integrated cavitation dose (ICD). Subsequently, the PNP-threshold for MBs stable and inertial cavitation regimes was identified using broadband emission (ICD^{BB}) as an indicator. In addition, the intracellular uptake of a fluorescent molecule was measured using flow cytometry over both PNPs regimes. The ICD over harmonics, ultra-harmonics and broadband were then correlated with the intracellular uptake with, and without considering MBs cavitation regimes.

Acoustic response of MBs depends on the PNP and tends to shift from stable to inertial cavitation with increasing PNP. The PNP-threshold at which MBs undergo inertial cavitation was 0.64 MPa. The ICD, overall, appeared to be independent of presence of cells. The percentage of FITC positive cells was greater within inertial cavitation regime compared to

stable cavitation regime. A weaker correlation within stable cavitation regime compared to that of inertial cavitation regime suggests that the correlation between the ICD and intracellular uptake may be dependent on MBs' cavitation regime. Nonetheless, under stable cavitation regime, a strong correlation of FITC positive cells with the 2^{nd} ultra-harmonic ICD indicates the potential of ICD to predict bio-effects induced by stable cavitation of MBs.

Several limitations of this study are the following: The experiments were performed in a cylindrical chamber made of mylar membrane. Thus, the issue of possible internal reflection was not considered in this study. Furthermore, the acoustic pressures at confocal region were measured in the absence of cylindrical chamber, which may have resulted in an underestimation of acoustic pressure at the confocal region. In addition, the ICD was not correlated with cell viability. Measuring cell viability will provide a better insight to this correlation and may provide a means to control acoustic bio-effects actively under various US exposure conditions. Furthermore, present study quantified cavitation activities of MBs as a function of exposure time only at varying PNPs. Similar characterization for a wide range of ultrasound parameters (e.g., frequency, pulse repetition period, pulse duration period, pulse sequencing, different MBs) would be useful because it will allow us to know whether the similar cavitation doses can be generated at different US conditions or not, if the same amount of acoustic energy is applied in a single treatment. Subsequent correlation with bio-effects may allow us to optimize US parameters to improve the efficacy USMB mediated therapeutic applications.

REFERENCES

[1] Baker, Kerry G., Valma J. Robertson, and Francis A. Duck. "A review of therapeutic ultrasound: biophysical effects." *Physical therapy* 81.7 (2001): 1351-1358.

[2] Chen, W. S., Matula, T. J., Brayman, A. A., & Crum, L. A. (2003). A comparison of the fragmentation thresholds and inertial cavitation doses of different ultrasound contrast agents. *The Journal of the Acoustical Society of America, 113*(1), 643-651.

[3] Chen, Wen-Shiang, et al. "Inertial cavitation dose and hemolysis produced in vitro with or without Optison®." *Ultrasound in medicine & biology* 29.5 (2003): 725-737.

[4] Chomas, James E., et al. "Threshold of fragmentation for ultrasonic contrast agents." *Journal of biomedical optics* 6.2 (2001): 141-150.

[5] Correas JM, Kessler D, Worah D, Quay SC (1997), The first phase shift ultrasound contrast agent: EchoGen. In: Goldber BB (ed) Ultrasound contrat agents. Dunitz, London, pp 83-99

[6] Cobbold, Richard S. C. *Foundations of Biomedical Ultrasound*. Oxford: Oxford UP, 2007.

[7] Coussios, Constantin C., and Ronald A. Roy. "Applications of acoustics and cavitation to noninvasive therapy and drug delivery." *Annu. Rev. Fluid Mech.*40 (2008): 395-420.

[8] Coviello, Christian, et al. "Passive acoustic mapping of stable and inertial cavitation during ultrasound therapy." *The Journal of the Acoustical Society of America* 136.4 (2014): 2300-2300.

[9] Datta, Saurabh, et al. "Ultrasound-enhanced thrombolysis using Definity® as a cavitation nucleation agent." *Ultrasound in medicine & biology* 34.9 (2008): 1421-1433.

[10] De Jong, Nico, et al. "Ultrasonic characterization of ultrasound contrast agents." *Medical & biological engineering & computing* 47.8 (2009): 861-873.

[11] De Cock, Ine, et al. "Ultrasound and microbubble mediated drug delivery: acoustic pressure as determinant for uptake via membrane pores or endocytosis." *Journal of Controlled Release* 197 (2015): 20-28.

[12] Dijkmans, P. A., Juffermans, L. J. M., Musters, R. J. P., Van Wamel, A., Ten Cate, F. J., Van Gilst, W., ... & Kamp, O. (2004). Microbubbles and ultrasound: from diagnosis to therapy. *European Journal of Echocardiography*, *5*(4), 245-246.

[13] Emmer, Marcia, et al. "Pressure-dependent attenuation and scattering of phospholipid-coated microbubbles at low acoustic pressures." *Ultrasound in medicine & biology* 35.1 (2009): 102-111.

[14] Erickson, Harold P. "Size and shape of protein molecules at the nanometer level determined by sedimentation, gel filtration, and electron microscopy."*Biological procedures online* 11.1 (2009): 32.

[15] Fan, Z., D. Chen, and C. X. Deng. "Improving ultrasound gene transfection efficiency by controlling ultrasound excitation of microbubbles." *Journal of Controlled Release* 170.3 (2013): 401-413.

[16] Fan, Zhenzhen, et al. "Spatiotemporally controlled single cell sonoporation."*Proceedings of the National Academy of Sciences* 109.41 (2012): 16486-16491.

[17] Ferrara, Katherine, Rachel Pollard, and Mark Borden. "Ultrasound microbubble contrast agents: fundamentals and application to gene and drug delivery." *Biomedical Engineering* 9 (2007).

[18] Forbes, Monica Mary. "The role of ultrasound contrast agents in producing sonoporation." *Doctor of Philosophy thesis in Bioengineering, Department of Bioengineering, University of Illinois at Urbana–Champaign, IL* (2009).

[19] Forbes, M. M., & Steinberg, R. L. (2008). Examination of inertial cavitation of Optison in producing sonoporation of Chinese hamster ovary cells. *Ultrasound in medicine & biology*, *34*(12), 2009-2018.

[20] Forbes, Monica M., Ryan L. Steinberg, and William D. O'Brien. "Frequency-dependent evaluation of the role of definity in producing sonoporation of Chinese hamster ovary cells." *Journal of Ultrasound in Medicine* 30.1 (2011): 61-69.

[21] Graham, Susan M., et al. "Inertial cavitation to non-invasively trigger and monitor intratumoral release of drug from intravenously delivered liposomes."*Journal of Controlled Release* 178 (2014): 101-107.

[22] Guzman, Hector R., et al. "Ultrasound-mediated disruption of cell membranes. II. Heterogeneous effects on cells." *The Journal of the Acoustical Society of America* 110.1 (2001): 597-606.

[23] Guo, Xiasheng, et al. "Investigation on the inertial cavitation threshold and shell properties of commercialized ultrasound contrast agent microbubbles."*The Journal of the Acoustical Society of America* 134.2 (2013): 1622-1631.

[24] Haak, Alex, and William D. O'Brien Jr. "Detection of microbubble ultrasound contrast agent destruction applied to Definity®." *Proceedings of the International Congress on Ultrasound*. 2007.

[25] Hafez, Zachary T. *The role of microstreaming in ultrasound-enhanced thrombolysis*. Diss. University of Illinois at Urbana-Champaign, 2008.

[26] Hallow, Daniel M., et al. "Measurement and correlation of acoustic cavitation with cellular bioeffects." *Ultrasound in medicine & biology* 32.7 (2006): 1111-1122.

[27] Helfield, Brandon, et al. "Individual lipid encapsulated microbubble radial oscillations: Effects of fluid viscosity." *The Journal of the Acoustical Society of America* 139.1 (2016): 204-214.

[28] Hoff, Lars. *Acoustic characterization of contrast agents for medical ultrasound imaging*. Springer Science & Business Media, 2001.

[29] Hwang, Joo Ha, et al. "Correlation between inertial cavitation dose and endothelial cell damage in vivo." *Ultrasound in medicine & biology* 32.10 (2006): 1611-1619.

[30] Kang, Shih-Tsung, et al. "Regulating nonlinear properties of lipid-coated microbubbles using polymer network scaffolds for ultrasound drug delivery applications." *Ultrasonics Symposium (IUS), 2014 IEEE International*. IEEE, 2014.

[31] Karshafian, Raffi, et al. "Sonoporation by ultrasound-activated microbubble contrast agents: effect of acoustic exposure parameters on cell membrane permeability and cell viability." *Ultrasound in medicine & biology* 35.5 (2009): 847-860.

[32] King, D. A., Malloy, M. J., Roberts, A. C., Haak, A., Yoder, C. C., & O'Brien Jr, W. D. (2010). Determination of postexcitation thresholds for single ultrasound contrast agent microbubbles using double passive cavitation detection. *The Journal of the Acoustical Society of America*, *127*(6), 3449-3455.

[33] Kiessling, Fabian, et al. "Ultrasound microbubbles for molecular diagnosis, therapy, and theranostics." *Journal of nuclear medicine* 53.3 (2012): 345-348.

[34] Lai, Chun-Yen, et al. "Quantitative relations of acoustic inertial cavitation with sonoporation and cell viability." *Ultrasound in medicine & biology* 32.12 (2006): 1931-1941.

[35] Lawrie, A., et al. "Microbubble-enhanced ultrasound for vascular gene delivery." *Gene therapy* 7.23 (2000): 2023-2027.

[36] Lentacker, Ine, et al. "Understanding ultrasound induced sonoporation: definitions and underlying mechanisms." *Advanced drug delivery reviews* 72 (2014): 49-64. A. Delalande,

[37] Liang, H. D., J. Tang, and M. Halliwell. "Sonoporation, drug delivery, and gene therapy." *Proceedings of the Institution of Mechanical Engineers, Part H: Journal of Engineering in Medicine* 224.2 (2010): 343-361.

[38] Liu, Yiyao, Hirokazu Miyoshi, and Michihiro Nakamura. "Encapsulated ultrasound microbubbles: therapeutic application in drug/gene delivery."*Journal of controlled release* 114.1 (2006): 89-99.

[39] May, Donovan J., John S. Allen, and Katherine W. Ferrara. "Dynamics and fragmentation of thick-shelled microbubbles." *Ultrasonics, Ferroelectrics, and Frequency Control, IEEE Transactions on* 49.10 (2002): 1400-1410.

[40] Miller, Douglas L., et al. "Bioeffects considerations for diagnostic ultrasound contrast agents." *Journal of Ultrasound in Medicine* 27.4 (2008): 611-632.

[41] Nassiri, D. K., and Hill, C. R. (1986). "The use of angular acoustic scattering measurements to estimate structural parameters of human and animal tissue," J. Acoust. Soc. Am. 79, 2048-2054.

[42] Nelson, Jared L., et al. "Ultrasonically activated chemotherapeutic drug delivery in a rat model." *Cancer research* 62.24 (2002): 7280-7283.

[43] Nyborg, Wesley L. "Basic physics of low frequency therapeutic ultrasound."*Ultrasound Angioplasty*. Springer US, 1996. 1-23.

[44] O'Reilly, Meaghan A., and Kullervo Hynynen. "Ultrasound enhanced drug delivery to the brain and central nervous system." *International Journal of Hyperthermia* 28.4 (2012): 386-396.

[45] Postema, M., Van Wamel, A., Lancée, C. T., & De Jong, N. (2004). Ultrasound-induced encapsulated microbubble phenomena. *Ultrasound in medicine & biology*, *30*(6), 827-840.

[46] Qiu, Yuanyuan, et al. "The correlation between acoustic cavitation and sonoporation involved in ultrasound-mediated DNA transfection with polyethylenimine (PEI) in vitro." *Journal of Controlled Release* 145.1 (2010): 40-48.

[47] Quaia, E. (2005). Physical basis and principles of action of microbubble-based contrast agents. In *Contrast Media in Ultrasonography* (pp. 15-30). Springer Berlin Heidelberg.

[48] Radhakrishnan, Kirthi, et al. "Relationship between cavitation and loss of echogenicity from ultrasound contrast agents." *Physics in medicine and biology* 58.18 (2013): 6541.

[49] Raisinghani, Ajit, and Anthony N. DeMaria. "Physical principles of microbubble ultrasound contrast agents." *The American journal of cardiology*90.10 (2002): 3-7.

[50] S. Kotopoulis, M. Postema, P. Midoux, C. Pichon, Sonoporation: mechanistic insights and ongoing challenges for gene transfer, Gene 525 (2) (2013) 191–199

[51] Sboros, V., et al. "The behaviour of individual contrast agent microbubbles."*Ultrasound in medicine & biology* 29.5 (2003): 687-694.

[52] Sboros, Vassilis. "Response of contrast agents to ultrasound." *Advanced drug delivery reviews* 60.10 (2008): 1117-1136.

[53] Schutt, Ernest G., et al. "Injectable microbubbles as contrast agents for diagnostic ultrasound imaging: the key role of perfluorochemicals."*Angewandte Chemie International Edition* 42.28 (2003): 3218-3235.

[54] Stride, E. P., and C. C. Coussios. "Cavitation and contrast: the use of bubbles in ultrasound imaging and therapy." *Proceedings of the Institution of Mechanical Engineers, Part H: Journal of Engineering in Medicine* 224.2 (2010): 171-191.

[55] Sun, Tao, et al. "Acoustic cavitation-based monitoring of the reversibility and permeability of ultrasound-induced blood-brain barrier opening." *Physics in medicine and biology* 60.23 (2015): 9079.

[56] Szabo, Thomas L., et al. "Determining the pulse-echo electromechanical characteristic of a transducer using flat plates and point targets." *the Journal of the Acoustical Society of America* 116.1 (2004): 90-96.

[57] Thomas, D. H., Butler, M. B., Anderson, T., Steel, R., Pye, S. D., Poland, M., ... & Sboros, V. (2009). Single microbubble response using pulse sequences: initial results. *Ultrasound in medicine & biology*, *35*(1), 112-119.

[58] Tung, Yao-Sheng, et al. "The mechanism of interaction between focused ultrasound and microbubbles in blood-brain barrier opening in mice." *The Journal of the Acoustical Society of America* 130.5 (2011): 3059-3067.

[59] Van Wamel, Annemieke, et al. "Vibrating microbubbles poking individual cells: drug transfer into cells via sonoporation." *Journal of controlled release*112.2 (2006): 149-155.

[60] Vaseghi, Saeed V. "Spectral Subtraction." *Advanced Signal Processing and Digital Noise Reduction*. Vieweg Teubner Verlag, 1996. 242-260.

[61] Vignon, Francois, et al. "Microbubble cavitation imaging." *Ultrasonics, Ferroelectrics, and Frequency Control, IEEE Transactions on* 60.4 (2013): 661-670.

Appendix

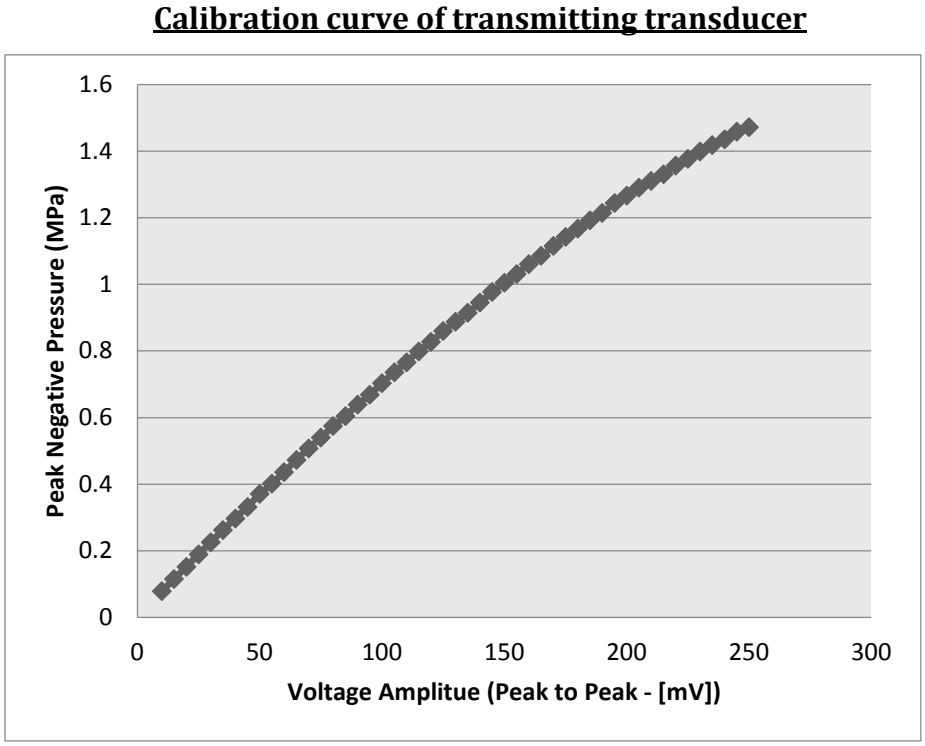

Figure A.1. The calibration curve of transmitting transducer 1.0 MHz used to determine acoustic pressures in the unit of Pascal at the focal region.

Table A.1. Characteristics of transmit and receive transducer

Transducers	Beamwidth [mm]	Fractional Bandwidth
Transmit Transducer 1.0 MHz	2.0 at FWHM	65% at FWHM
Passive Transducer 2.25 MHz	2.0 at FWHM	75% at FWHM